Investigation of Activated Biochar from Water Hyacinth for Removal of Iron from Steel Industry Wastewater

Sofia Sultan Hussein

Department of Chemical Engineering

School of Mechanical, Chemical, and Materials Engineering

Presented in Partial Fulfillment of the Requirement for the Degree of Master's in Chemical Engineering (Specialization in Process Engineering)

Office of Graduate Studies

Adama Science and Technology University

Adama, Ethiopia

January, 2023

Investigation of Activated Biochar from Water Hyacinth for Removal of Iron from Steel Industry Wastewater

Sofia Sultan Hussein

Advisor: Dr. Selvakumar Periyasamy

Co-Advisor: Dr. Zelalem Tumsa

A Thesis Submitted To

The Department of Chemical Engineering

School of Mechanical, Chemical, and Materials Engineering

Office of Graduate Studies

Adama Science and Technology University

Adama, Ethiopia

January, 2024

Declaration

I declare that the thesis/ dissertation proposal entitled “Investigation of activated biochar from water hyacinth for removal of the iron from steel industry wastewater” for the M.Sc. degree at the University of Adama Science and Technology, hereby submitted by me and has not previously been submitted for a degree at this or any other university and that all resources of materials used for this thesis proposal have been duly acknowledged.

Sofia Sultan		
Name	Signature	Date

Advisors Approval Sheet

We here certify that the recommendation and suggestion given by the proposal review committee are appropriately incorporated into the final thesis proposal entitled “Investigation of Activated Biochar from Water Hyacinth for Removal of Iron from Steel Industry Wastewater” by Sofia Sultan.

1. Dr. P. Selvakumar	_____	_____
Major Advisor	Signature	Date
2. Dr. Zelalem Tumsa	_____	_____
Co-Advisor	Signature	Date

Approval Page

We, the undersigned, members of the Board of Examiners of the thesis by Sofia Sultan Hussein have read and evaluated the thesis entitled “Investigation of Activated Biochar from Water Hyacinth for Removal of Iron from Steel Industry Wastewater’’and examined the candidate during the open defense. This is, therefore, to certify that the thesis is accepted for partial fulfillment of the requirement of the degree of Master of Science in Chemical Engineering.

Chairperson	Signature	Date
Internal Examiner	Signature	Date
Dr.Sintayehu Mekuria		
External Examiner	Signature	Date

Finally, approval and acceptance of the thesis is contingent upon submission of its final Copy to the Office of Postgraduate Studies (OPGS) through the Department Graduate Council (DGC) and School Graduate Committee (SGC).

Department Head	Signature	Date
School Dean	Signature	Date
Office of Postgraduate Studies, Dean	Signature	Date

Acknowledgement

First, I would like to thank the almighty God for the strength and good health that allowed me to complete this thesis work. Then, I would like to transfer my special thanks and gratitude to my advisors Dr. P. Selvakumar and Dr. Zelalem Tumsa for their continuous guidance, indispensable comments, encouragement, support, and excellent supervision throughout my research work. Thank you for generously sharing your time, and for all your support to succeed in this research.

I would like to thank Mr. Demeke (senior lab assistant) for his valuable guidance, and for kindly supporting me in completing the laboratory analysis work at the materials Science engineering department of Adama Science and Technology University. My thanks to all Academic and Research Assistants of the Chemical Engineering Department, at Adama Science and Technology University. This thesis would not have been possible without the inspiration and support of several wonderful individuals. Thank you all of my friends specially Melat Mechal for being part of this journey and making this thesis possible.

Finally, my deep and sincere gratitude to my whole family member. Your endless support, encouragement, appreciated sacrifice, and constant love have sustained me in success throughout my life.

Table of Contents

List of Figures

List of Tables

List of Acronyms

AAS	Atomic Absorption Spectroscopy
AC	Activated carbon
ASTU	Adama Science and Technology University
BC	Bio-char
BET	Brunauer-Emmett-teller
DTA	Differential thermal analysis
FTIR	Fourier-Transform Infrared Spectroscopy
KOH-AC-WHBC	potassium hydroxide activated waterhyacinth biochar
Kf	Freundlich adsorption capacity (mg/g)
kf	Pseudo first order rate constant
KL	Langmuir equilibrium constant (l/mg)
Ks	Pseudo second order rate constant
n	Sorption intensity
qm	Monolayer sorption capacity at equilibrium (mg/g)
qe	Amount of sorbate sorbed at equilibrium per unit mass (mg/g),
SEM	Scanning Electron Microscopy
TGA	Thermo-gravimetric analysis
UV	Ultraviolet–visible
WHBC	Water hyacinth-derived biochar
WHO	World health organization
XRD	X-ray Diffractometer

Abstract

This study investigated the removal of heavy metal ions from industrial wastewater by water hyacinth biochar. The choice of the materials was influenced by their large surface area, abundance of functional groups as well as their availability in the local environment. The development of environment-friendly natural adsorbents to treat heavy metal, contaminated wastewater stands as a foremost area of investigation, due to its environment-friendly nature. In the present experimental investigations "the adsorption of iron against an aqueous mixture utilizing chemically activated water hyacinth is studied batch-wise". Adsorption capability in the elimination of iron metal ions has been examined by various influencing criteria such as pH, time of contact, initial ion concentration, and adsorbent dosages. This study is done to find a cost-efficient adsorbent as well as understand the process aimed at the removal of heavy metal in wastewater with the aid of the lignocellulose plant adsorbent. Activated biochar prepared from water hyacinth is made using a chemical activation technique. The adsorption of Fe (II) ions onto potassium hydroxide-activated carbon derived from water hyacinth root (KOH-AC-WHL) is described. KOH-AC-WHL was characterized using UV spectroscopy, XRD, SEM, BET, and FT-IR spectrometry. The adsorption kinetics showed a better fit with the pseudo-second-order kinetics model with a good linear correlation coefficient (R^2) value of 0.998 compared to the (R^2) value of 0.712 for a pseudo-first-order kinetics. The Langmuir and Freundlich models were used to fit the adsorption experimental data. A better correlation with the Langmuir model was observed with an (R^2) value of 0.987 compared to the (R^2) value of 0.97 for the Freundlich model. Hence, the maximum adsorption capacity of the adsorbent for Fe (II) ions was calculated from the Langmuir isotherm and found to be 312.5 mg/g. The reusable efficiency of KOH-AC-WHBC was found to be 68% after four consecutive cycles.

Keywords: *Water hyacinth biochar, Adsorption, Cost-efficient, Efficiency, Heavy metal, iron removal*

Chapter One

1. Introduction

1.1. Background

Wastewater management is one of the most important social and environmental problems in emerging countries These issues are brought on by urbanization, rapid population growth, increased need for industrial development, and a lack of resources to handle the rising volume and declining quality of wastewater produced in the majority of these developing countries(Connor et al. 2017).

Pollutants in wastewater are dangerous to both human and environmental health. Pathogenic bacteria, nutrients including phosphate and nitrogen, hydrocarbons, organic matter, endocrine disruptors, and heavy metals are examples of pollutants that pose a risk to human health and the environment(Olaolu et al., 2014). Wastewater containing these contaminants is produced by a variety of human activities, including mining, agriculture, residential waste, urban runoff, and effluents from wastewater that has not been properly treated using standard treatment units (Group, 2016).

Because they are not biodegradable and have a propensity for bioaccumulation in living things, heavy metals are a serious concern(Arora, 2019). Limited levels of heavy metals including Fe, Co, Cu, Mn, and Zn are necessary for the physiological operation of living things. However, these metals turn harmful when they reach the maximum allowable limits (Olaolu et al., 2014). Additionally, some heavy metals, such as Hg, Cr, and Pb can be found in the environment in various speciation and are extremely harmful to species. Some heavy metals, such as Cr, exist in two states: the less harmful Cr (III) and the more poisonous Cr (VI), whereas Fe is found in both the ferrous (Fe (II)) and ferric (Fe (III)) states(Tchounwou et al., 2012). Therefore, proper and cost-effective methods to reduce their concentration or limit their presence and mobility in wastewater are highly needed.

Heavy metals from industrial wastewater have been removed using a variety of procedures, including lime precipitation, ion exchange, adsorption onto activated carbon, membrane processes, and electrolytic approaches (Barakat, 2011). These techniques are, however, limited because they frequently come with substantial capital and operational costs in terms of power

consumption and required working hours. Additionally, typical wastewater treatment methods call for specialized knowledge and generate a lot of sludge (Rwiza et al., 2018). Recently, there has been more focus on safe and cost-effective alternative methods for the elimination of heavy metals from wastewater to complement the commercially available approaches. Apart from the various advantages of these technologies they have major drawback being energy intensive and not ecofriendly. Adsorption technique by using naturally available waste is considered as best alternate for removal of heavy metals. Hence, adsorption technique using a naturally modified adsorbent is more efficient, feasible and ecofriendly compared to other conventional processes and the possibility of reusing the spent adsorbent.

Water hyacinth is a floating recurrent herbaceous plant native to South America Amazon river basin, found throughout the world and introduced to Ethiopia in 1965 (R. Zhou et al., 2020). It grows and reproduces quickly, causing navigation jams, interfering with irrigation, fishing, and power generation; blocking sunlight penetration; lowering water dissolved oxygen (DO) concentration; competitively excluding submerged plants; and reducing biological diversity (Y. Huang et al., 2014). Activated carbon production from water hyacinth is considered an appropriate technology to obtain efficient adsorbents at low cost, and also has a high surface area and enriched functional groups, with the goal of controlling the water hyacinth invasive weed and solving environmental pollution problems.

In Ethiopia, there are mitigation efforts, research studies and stakeholder activities to control the spread of the WH. The efforts have not been effective due to different reasons and the management or control were also unsuccessful. Some of the reasons were low efficiency of mechanical removal work, shortage of scientifically acceptable dumping site, and limited cooperation by local community members. To enact community participation approach for controlling the WH, studies suggest some methodologies such as empowering opportunities and enticing the locals with potential economic gains (Honlah et al., 2019). Ethiopia has a conservation responsibility for the east African water ecology. Inevitably, the country's fresh water bodies have seriously been affected by the invasive water plants such as WH, which need continued efforts. The nature of the climate of Sub-Saharan Africa and the prevailing weather conditions, particularly hot environments, in the Ethiopian rift valley lakes favor the proliferation

and quick expansions of the WH plant in the regions. Additionally, there is eutrophication due to flooding from the farmland that brings artificial fertilizer enter in to the lake water body.

Various activated carbon from water hyacinth leaf was used for the adsorption of Fe(II), and a lower adsorption capacity was reported (Y. Huang et al., 2014). It may need other activation methods and chemicals to enhance the removal efficiency of Fe(II) ions. Hence, KOH-activated carbon from water hyacinth root is prepared, and the adsorption capacity of Fe(II) was studied by optimizing various parameters like pH, adsorbent dosage, contact time, and initial Fe(II) ions concentration using batch experiments. The obtained adsorption capacity (312.5 mg/g) is higher than ever reported using water hyacinth based materials for Fe(II) ions removal.

The WH control and management needs an integrated approach involving community participation than just mechanical eradication. Assessing WH socioeconomic and environmental impact for the better management of water habitats is vital, particularly, at upper Awash River Basins of the rift valley lakes in Ethiopia. Therefore, water hyacinth-based biochars were used in this study to remove selected inorganic pollutants from industrial wastewater. Water hyacinth was chosen as precursor material because of the perspective of environmental, economic, and social perspective in Ethiopia, where the study was carried out.

1.2. Statement of the Problem

Wastewater management has become one of the significant social and environmental challenges in developing countries. Heavy metals are of significant concern because they are non-biodegradable and have a tendency to bio-accumulate in living materials (Lakherwal, 2014). Iron is among these heavy metals which are released from the steel industry. Initially, concentrations above 0.3 mg/l level, in drinking water may not have adverse health effects. However, continuous consumption of such water with elevated levels of iron may result in a condition called iron overload. Excessive iron intake may lead to the impairment of hematopoiesis by destroying the progenitor cells as well as the microenvironment for hematopoiesis. If iron overload is left untreated, it may lead to hemochromatosis, which damages different organs of the body. Initial symptoms include weight loss, joint pain, and fatigue. Eye disorders such as retinitis, conjunctivitis and choroiditis, cancer, and heart diseases are also some of the common health issues faced due to high concentrations of iron in the water.

Total iron removal technologies and percent removal including electro-coagulation (EC) 95–99%, oxidation/filtration 80–90%, ion exchange 90%, adsorption–oxidation 84–92%, activated carbon filtration 75–90%, subsurface iron removal more than 50%, aerated granular filter 80–90%, bioremediation 70%, supercritical fluid extraction 80% have been developed for removal of total iron from municipal and industrial effluents (Chaturvedi & Dave, 2012). Apart from the various advantages of these technologies, they have major drawbacks being energy intensive and not ecofriendly. Adsorption technique by using naturally available waste is considered the best alternative for the removal of heavy metals. Hence, the adsorption technique using a naturally modified adsorbent is more efficient, feasible, and eco-friendly compared to other conventional processes.

Only a few studies have focused on the characteristics of bio-chars from Eichornia crassipes (water hyacinth) (Masto et al., 2013). The aggressive invasion of E. crassipes destroys many ecologically and economically important water bodies and productive wetlands by starving the water of oxygen and destroying native biodiversity (Téllez et al., 2008). As a result of its high reproductive rate and dispersion, E. crassipes has been identified by the International Union for Conservation of Nature as one of the 100 most cumbersome invasive species and one of the top 10 worst weeds in the world (Patel, 2012). Currently, the main treatment method for E. crassipes is its physical removal from water bodies; however, this treatment has minimal effect (Téllez et al., 2008). Due to the property of excessive reproduction in unhealthy aquatic ecosystems, *E. crassipes* can serve as a potential ecological indicator for heavy metal contaminants either at low- or high-level contamination.

1.3. Basic Research Questions

1. Is it possible to activate by using potassium hydroxide on the surface of water hyacinth-derived biochar to synthesize effective adsorbent for iron removal?
2. What is the role of potassium hydroxide in the development of an adsorbent to remove iron from wastewater effluent?
3. What would be the effect of synthesizing factors (i.e. calcination temperature and time) and optimum parameters (i.e. pH, adsorbent dose, initial concentration, and contact time) for iron removal?

Based on the above research questions the choice of the systems is formed as follows;

Adsorption, water hyacinth-derived biochar are selected as a base and focal point due to: (1) adsorption technology is effective for removing iron from wastewater, even at low concentrations, among the chemical, physical, and biological methods, (2) water hyacinth-derived biochar is among the most promising low-cost, environmentally friendly, readily available, and effective adsorbents and has recently received a lot of interest in practical application, and (3) water hyacinth as a renewable and sustainable source will provide inexpensive and environmentally friendly bioproducts.

1.4. Objective

1.4.1. General Objective

- Synthesis of activated biochar synthesis from water hyacinth for the removal of iron from steel industry wastewater

1.4.2. Specific Objective

- Prepare, treatment, and characterize water hyacinth physiochemical property and bio-char from water hyacinth
- Investigating and evaluating batch adsorption experiment to study the effect of operating parameters(adsorbent dose, initial iron concentration, pH of the solution, and contact time) for iron removal efficiency of activated biochar from synthetic wastewater
- Determine equilibrium and kinetic parameters of adsorption of iron by modified bio-char by applying some commonly used adsorption isotherms and kinetic models and study the adsorbent regeneration
- Investigate the effect of other competitive ions on iron removal efficiency of activated bio-char in real steel industry wastewater in the optimum operational conditions

1.5. Significance of the Research

This study has the potential to benefit both the environment and human health. Environmental remediation such as heavy metals (iron) which are toxic to humans and the environment by using abundant biomass water hyacinth which is an invasive aquatic plant that grows rapidly in water bodies. So that we can turn this invasive species into a valuable resource (biochar) for mitigating heavy metal pollution means simultaneously addressing two environmental issues: invasive species control and pollution remediation. When water hyacinth is converted into biochar, it can become an effective and sustainable means of removing heavy metals from contaminated water.

This makes it a cost-effective and sustainable solution for communities and regions found in Ethiopia with heavy metal contamination.

1.6. Scope of the Study

This study focuses on synthesize of activated biochar using water hyacinth and also understand the characteristics of adsorbent to remove Fe(II) metal from aqueous solution and determine under what optimum condition it gives maximum removal efficiency concerning pH, a dosage of adsorbent, the effect of contact time and initial concentration in batch system and finally determine kinetics and isotherm using model equations available in the literature and reusability of the adsorbent were studied. Not only the effect of co-existing ion within iron ion but also the performance of the activated biochar for real water studied in this work.

Chapter Two

2. Literature Review

2.1. General View of Heavy Metal

Inorganic and organic substances that can dissolve in water, such as pesticides, pharmaceuticals, heavy metals, petroleum products, dyes, and other contaminants, have contributed to an increase in the problem of global water pollution (Hoang et al., 2021), and a lack of freshwater for human consumption(Le et al., 2021) has made it difficult to find effective water treatment methods. Heavy metals are the water contaminants that have the most harmful effects on the environment anywhere in the globe (Vardhan et al., 2019). According to Beni and Esmaeili (2020), heavy metals are mostly released into the environment by large-scale enterprises such as those that produce leather, metal, petroleum, batteries, textiles, fertilizers, nuclear power, and pesticides.

Unfortunately, even at low concentrations, heavy metals cannot be biodegraded, leading to bioaccumulation inside living things(Hoang et al., 2022). Organ damage, stillbirth, cancer, skin conditions, migraines, mental retardation, growth retardation, and nervous system dysfunction have all increased in frequency as a result (J. Wang et al., 2021). The negative effects of toxic waste could be reduced by removing heavy metals from environmental water and wastewater (Hoang et al., 2021).

Fig. 2.1 illustrates different investigations to remediate heavy metals as well as some methods in use with both pros and cons that include leaching (Y. Zhang et al., 2017), solvent extraction, reduction, ion exchange, oxidation, and bioremediation (Shah et al., 2017), adsorption, membrane filtration, and electrochemical treatment (Hoang & Pham, 2021). Among the above-mentioned approaches, adsorption has extensively been used for treating heavy metal-aqueous systems due to its simple process, easy scalable, low expenses, versatility, and wide range for pH working (Moradi & Zare, 2013).

A variety of adsorbent materials have been developed for a few decades (Rattanaphan et al., 2020), and several of those compounds were efficient in eliminating target pollutants as well as successful in larger-scale applications. Because of the limitations in technology and heterogeneities of applications, practically only a small number of these novel materials could be scale-up (Zeng et al., 2019). With the use of bio-adsorbents derived from waste biomass, several

environmental issues and cost problems related to other kinds of treatments could be addressed (Chau et al., 2021). More noticeably, a porous solid during adsorption had a high proportion of surface area to volume/mass as well as a variety of surface functional groups were able to link to aqueous metals through chemisorption, physisorption, and several combinations.

In actuality, one of the functions of metal types and functional groups, a specific region of the surface, and other adsorbent characteristics was the binding type; however, the drawbacks of these materials included challenges in manufacturing and demands for pricey chemicals and machinery. Due to this, biochar, which is produced alongside bio-oil and gases when biomass is roasted to a high temperature without the presence of oxygen, has lately been investigated as an adsorbent. As a result, biochar which is generated besides bio-oil and gases in pyrolysis where biomass is heated under high temperature without the presence of O_2 has recently been studied as adsorbents. In particular, the temperature of pyrolysis is in the range of 300–900 °C with the solid residence times from seconds to minutes/hours and a liquid is produced in the process (Papari et al., 2015). Moreover, pyrolysis also uses a range of feedstock such as agricultural residues (Sahoo et al., 2021), woody biomass (Ding et al., 2019), and sewage sludge (Zaker et al., 2019).

Indeed, biochar possesses special properties including low expense, high performance, and fewer effects on the environment (Yavari et al., 2017), so it has received more attention currently as an alternative to conventional carbon-based materials, namely graphene oxide, carbon nanotubes, and activated carbon (Lian et al., 2019). However, activation progression is normally required in producing activated carbon, which leads to the additional expense of production, while this process is unnecessary in generating biochar which is also far simpler (Lian et al., 2019).

There has been limited research on "designed biochar" to manage contaminants, especially for "potentially toxic elements," even though biochar materials have been examined to scavenge pollutants in a water body (Premarathna et al., 2019). The majority of those studies emphasized the capacity of adsorption of biochar materials towards inorganic or organic pollutants, namely how biochar was applied in storm water (Mohanty et al., 2018), biochar-supported nZVI (S. Wang et al., 2019c), biochar modification potential (Rajapaksha et al., 2016), and biochar for purifying drinking-water (Beni & Esmaeili, 2020). The aforementioned publications primarily

concentrated on pristine biochar which was generated from single-source biomass as well as how it was used to improve soil fertility or remove contaminants.

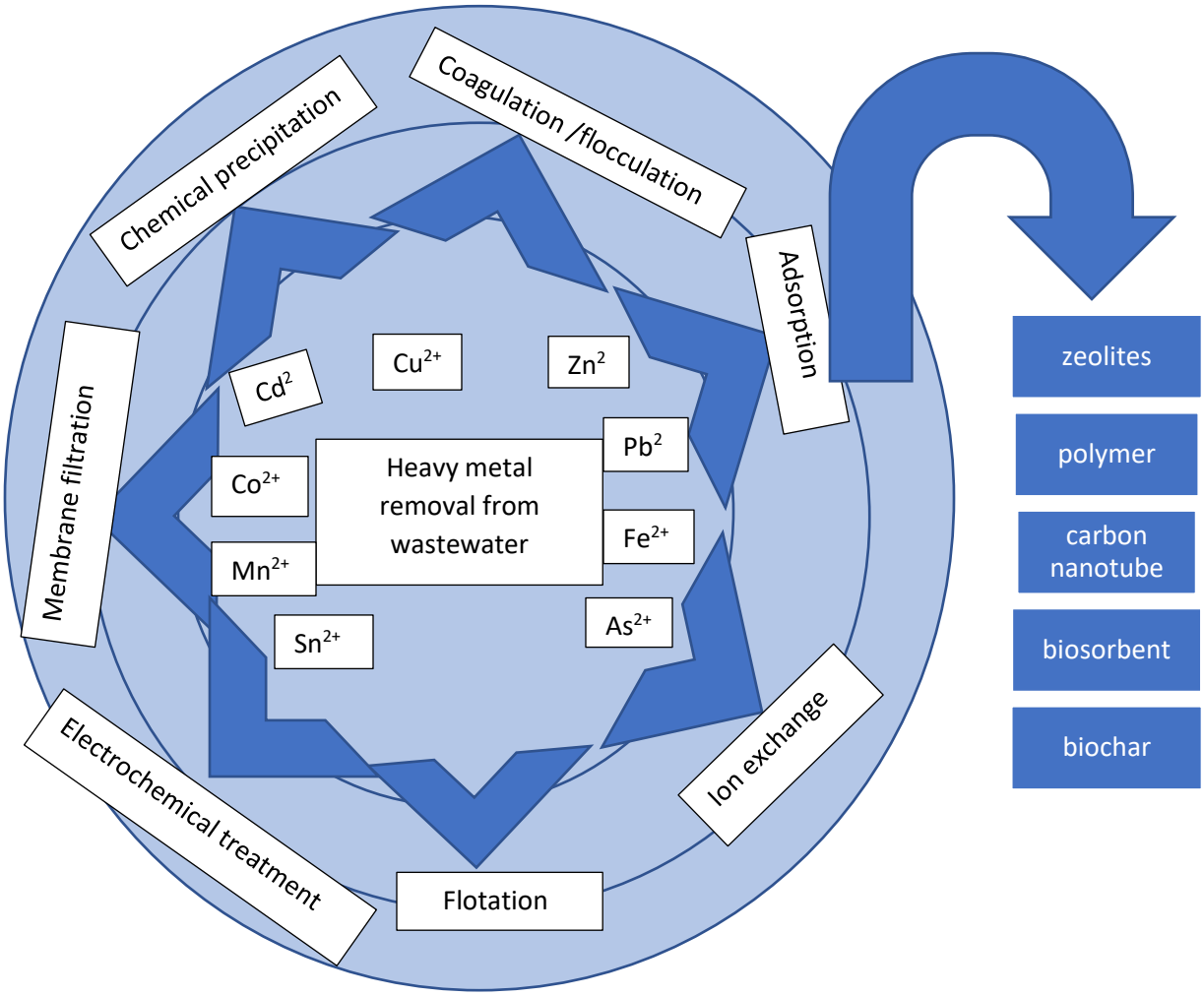

Figure 2. 1: Various methods for heavy metal adsorption (M. Yadav & Yadav, 2015)

Table 2.1 presents a comparison of the various methods available for removing heavy metal pollution from water. The table indicates that adsorption is widely used in the treatment of heavy metal ions owing to its advantages, such as simple operation, high removal rate, strong applicability, and low cost of reusable adsorbents (Z. Li et al., 2020), and currently the most promising method for controlling heavy metal pollution. The most important consideration in the adsorption technology is the selection of suitable adsorbents. A good adsorbent should have attributes, such as a large specific surface area, fast adsorption rate, and short equilibrium time (Cai et al., 2019). From this perspective, bio-char stands out from many new functional materials

used for environmental applications as a highly efficient adsorbent, owing to its low price, wide source of materials, and lack of ecological impact.

Table 2. 1: The Methods Comparison for Removing Heavy Metal Pollutants from Polluted Water.

Method	Technical maturity	Cost	Pollution environment	automaticity	Refs.
Chemical Precipitation	Mature	High	Higher	high	(M. Kumar et al., 2021)
Electrochemical	Lower	High	Low	higher	(Martínez-Huitle & Panizza, 2018)
Redox	Low	Low	Lower	low	(Hu et al., 2020)
Iron exchange	Lower	Higher	Lower	high	(Dąbrowski et al., 2004)
Adsorption	High	Low	Low	lower	(Burakov et al., 2018)
Membrane separation	Higher	Higher	Low	lower	(Abdullah et al., 2019)

2.1.1 Iron Removal Strategies

Iron removal efficiency, merits, and demerits of each method have been depicted in Table 2.2

Table 2. 2 :- Method for Iron Removal with Their Respective Merit, Demerits and Efficiency

Method	Merits	Demerits	Efficiency (%)	Cost	Ref.
Conventional Strategies Oxidation-precipitation-filtration process	• Simple operation • Oxidant used kills the harmful disease-causing	•Corrosion of parts of the system by the oxidant	90–95	Low	(Boyle et al., 1977)

	bacteria present in water				
Zeolite softening/Ion exchange	•Effective removal of organic iron Zeolite can be reused after regeneration	•Clogging due to oxidation .• Labor-intensive cleaning of the system after clogging	65–85	Low	(Bulai & Cioanca, 2005)
Calcium carbonate-based materials	•No effect of temperature or flow rate on the efficiency of the process •High removal efficiency	•Reduced efficiency in the presence of co-cations and natural organic matter (NOM), lower pH, and large-sized materials	94–99	Low	(Shavandi et al., 2012)
Filter media separation	• Fast rate •No need for chemicals • Back washing is a necessity • Effective for removing pathogenic microbes	•Back washing is a necessity •Ineffective for removing inorganic iron	90–98	Low	(El-Naggar, 2010)
Removal through supercritical fluid	• Increased removal efficiency at longer contact time between chelating agent and iron	•Complex process	79–85	High	(Andersen & Bruno, 2003)
Solid sorption separation/Adsorption	• Low cost	•Ineffective to remove pathogenic microbes	77–90	Low	(Tahir & Rauf, 2004)
Wetland treatment	•No use of chemicals • Increased efficiency at higher loading rates	• Low removal efficiency Low •Ineffective for removing high concentrations of iron	40–80	Low	(Johnson & Younger, 2006)

	• Effective for co-treatment of water from different sources				
Electrocoagulation and Electrocoagulation/ flotation	.Simple equipment • Easy operation • High removal Efficiency	• Ineffective at lower pH • Requirement of high current densities	95–99	Low	(Ghosh et al., 2008)
Aeration	• No need for chemicals • Good mixing	•High residence time •In efficient oxidation of Fe^{2+} in the absence of an airlift reactor.	40–90	Low	(Štembal et al., 2005)
Sequestration process	•Easy operation •No production of residues	•Low efficiency •Reduced efficiency with alkaline and hard water	66	Low	(Volpe et al., 2012)
Biological Strategy	•High specificity due to different bacterial strains •High efficiency •No need for chemicals	•Only suitable for neutral pH condition • Requirement of long start-up time by microbes on the biofilter	93–96	Low	(Volpe et al., 2012)
Membrane technology-based Strategy	•Less retentive volume • Minimum labor requirement	• Membrane fouling • Reduced efficiency after a few cycles of operation	95–98	High	(Choo et al., 2005)
Nanotechnology-based Strategy	• Highly selective • High efficiency	• Toxicity of nanoparticles • Difficulty in removal from water due to Nano-scale size	99	High	(Alimohammadi et al., 2017)

2.2 Water Hyacinth as a Biomass

Eichhornia crassipes, also known as water hyacinth (WH), is one of the world's most problematic aquatic plants and a member of the Pontederiaceae family (Neris et al., 2019). Many photosynthetic species depend on sunlight penetration, which can be reduced by the formation of WH on the water's surface. Therefore, WH reduces the growth rate of photosynthetic organisms, upsetting the ecological balance. The removal of HM ions from aquatic ecosystems by particular aquatic plants is being investigated with increasing interest (vlyssides et al., 2001). WH has the potential to remove aquatic pollutants (Rezania et al., 2015), which reduces its negative environmental impact (Da Silva Correia et al., 2018). (Du et al., 2020) reported that WH not only accumulates a wide range of HMs (i.e., non-selective uptake), but it also enhances their uptake and translocation in the more polluted areas, demonstrating that it has a strong ability for HM removal from water.

Due to its qualities, including its high rate of growth, effectiveness in absorbing pollutants, cheap operating costs, and renewability, WH is a good candidate for phytoremediation in the treatment of wastewater, including home and industrial effluents (Rezania et al., 2015). In addition, (Sanmuga Priya & Senthamil Selvan, 2017) reported that WH is suitable for use in wastewater treatment due to its high biomass production rate, high pollution tolerance, and heavy metal and nutrient absorption abilities. Since WH comprises a sizable amount of cellulose (35%) and hemicellulose (30%), it can be used as an option to treat water that has been contaminated with HMs. Adsorbents are developed for HM removal based on the metals' interactions with the functional groups in the adsorbents. Thus, the presence of hydroxyl (OH), amino (NH_2), and carboxyl (C=O) groups in the cellulose enables the adsorption of different HMs by cation exchange.

WH biomass that has been dried and crushed has removed around 70% of the HMs from contaminated water in laboratory studies (Carreño-Sayago, 2021). The HM cations and the oxygen of the OH group in the vegetal cellulose of WH can share a pair of electrons. The chemical or physical modification of WH biomass is one method for maximizing HM elimination (Carreño-Sayago, 2021).

(Zhu et al. 1999)demonstrated the potential of WH biomass for the phytoremediation of As (V), Cd (II), Cr (VI), Cu (II), Ni (II), Fe (II), and Se (VI) under controlled conditions. The highest

accumulation was found for Cd and Cr, there were moderate levels of accumulation for Se and Cu, and the lowest level of accumulation was for As and Ni. They concluded that WH biomass had high bioconcentration factors for the studied elements when exposed to low concentrations of these elements. (Lu et al., 2004) concluded that WH biomass was a moderate accumulator of Cd and Zn and can be beneficial in treating water contaminated with low levels of HMs. Kabata-Pendias and Mukherjee (2007) mentioned that WH has a strong ability to accumulate heavy metals.

Mahamadi and Nharingo (2010) used WH biomass in a batch sorption experiment to study the biosorption of Cd^{2+}, Pb^{2+}, and Zn^{2+} ions in binary and ternary systems under acidic conditions (pH = 4.84) and a temperature of 30 °C. The mixed action of these metals was found to be incompatible following the order $Pb^{2+,}Cd^{2+}$ and Zn^{2+} while competitive biosorption behavior was recorded for the combinations Pb–Cd and Pb–Zn as described by the Langmuir competitive model. They concluded that Pb^{2+} ions could be efficiently eliminated from aqueous solution in the occurrence of Cd^{2+} and Zn^{2+} ions, but the elimination of the Cd^{2+} and Zn^{2+} ions would be repressed in the presence of Pb^{2+}. (Neris et al., 2019) conducted kinetic and isotherm investigations of Pb^{2+}, $Ni^{2+,}$ and Zn^{2+} ions adsorption in single and tri-element aqueous systems using modified alkali-treated WH biomass because of its higher ion adsorption capacity than acid-treated WH biomass and WH biomass washed with water Analysis by FTIR confirmed that −OH and −COO− groups were the key functional groups in Zn^{2+} adsorption, while −COO− groups were key in Pb^{2+} and Ni^{2+} biosorption. The pseudo-second order was the best kinetic model that fit the single and tri-element experimental data for all investigated ions.

The selectivity order of WH in single and tri-element systems was $Pb^{2+} >> Zn^{2+} \geq Ni^{2+.}$ (Hemalatha et al., 2020) studied the remediation of Zn and Cr ions from electroplating industry wastewater by dried WH biomass (leaves, petiole, roots) through batch and column experiments. They considered influential parameters including biosorbent dosage, initial concentration of HMs, initial pH, and contact time. The WH root showed maximum Zn removal of 98.9%, and WH stem showed Cr removal of 96.4%. Thus, the results indicated that the dried WH biomass was a good and low-cost adsorbent.

Therefore, WH is a promising and potentially ecofriendly method of HM remediation from aqueous solutions. However, this needs more study because most of the previous research

confirmed that surrounding conditions control the removal percentage, and this percentage differs among metals.

2.3. Water Hyacinth Biochar

WH biochar has been used in many applications, such as adsorbing HMs, as a soil amendment, and for bioenergy production (Allam et al., 2020). Converting WH tissues into biochar to remediate wastewater could be a win-win strategy for both removing pollutants and the effective management of a highly problematical invasive species (Yu et al., 2018).

WH biochar has a nonhomogeneous, coarse, and porous surface that has many different (in size, shape, and depth) pores (Allam et al., 2020). The microspores in the surface of WH biochar are produced during the pyrolysis process when substances are volatilized; the volatiles are trapped in the biomass and expand its microstructure. WH biochar has displayed potential for HM adsorption from different types of wastewater (C. Liu et al., 2020).

The use of WH biochar for HM removal is the most recent and focused trend as a profitable pathway for the use of WH (Gaurav et al., 2020). The WH biochar generated at different pyrolysis temperatures had shown promise for high removal efficiency of HMs such as Cd with biochar created at 300, 500, and 700 °C (C. Liu et al., 2020) and Cu^{+2} and Zn^{+2} with biochars created at 300 and 600 °C (Nyamunda et al., 2019). A significant challenge with the use of biochar in aqueous solutions is its low density in powdered form(C. Liu et al., 2020). Some researchers overcame this problem using modifications such as alginate capsules (Nyamunda et al., 2019) or magnetic modification (C. Liu et al., 2020). This is a promising way to sustainably utilize this invasive plant (C. Liu et al., 2020). Use with algae is another option to increase the efficiency of WH biochar (Shen et al., 2018).

2.4. Biochar Production and its Properties

2.4.1. Typical Methods for Biochar Production and Formation Mechanism

Biomass, with its high carbon content, is a renewable energy source in the form of highly active bio-char upon thermos-chemically processing. Pyrolysis has attracted significant interest in the past few years as one of a small number of well-established thermochemical processes for treating biomass as well as bio-derived waste for the high yield of energy char along with oil and gas (Chau et al., 2021). Factors in the process had a significant impact on the pyrolysis products'

dispersion and efficiency, especially pyrolysis process factors such as residence duration, heating rate, and temperature all affected bio-char generation (Tripathi et al., 2016). Some of the bio-char production approaches are hydrothermal carbonization, gasification, pyrolysis, and others. An overview of different methods of producing bio-char and various conditions of operation

2.4.1.1. Gasification

The process of conventional carbon utilization was only able to transform a part of carbon, meanwhile, the whole carbon elements that were present in biomass feedstock could be directly converted into wanted outputs (e.g. syngas including CO and H_2, bio-oil, and bio-char) through the thermochemical progression such as pyrolysis and gasification (Ben et al., 2019). Consequently, to transform recalcitrant carbon (namely lignin) into value-added outputs, an effective approach was thermochemical biomass conversion (Mao et al., 2019).

Being a thermochemical conversion method, gasification aimed to create gaseous fuels from carbon types in biomass with the use of a catalyst or oxidant at high temperature, whereas under pretty lower temperature conditions, solid, liquid, and gaseous products could be produced in pyrolysis (Yaashikaa et al., 2020). It is clear that in the process of gasification, the temperature was an important factor as high temperature enhanced the production of CO and H_2 while reducing CO_2, and CH_4 (Prabakar et al., 2018). In comparison with the bio-char in pyrolysis, bio-char in gasification had a smaller surface area and contained fewer functional groups (e.g. carboxyl, carbonyl, and hydroxyl groups) (Peterson and Jackson, 2014).

2.4.1.2 Pyrolysis

The pyrolysis process with a temperature of more than 300 °C without O_2 caused the organic components in biomass to thermally decompose (Mohan et al., 2006). The process also released the vapor phase and created residual solid-phase bio-char materials. When the vapor phase was cooled down, bio-based oil was generated, in which the blend of high-molecular-weight organic and polar composite experienced condensation (Chua et al., 2019). Meanwhile, low-molecular-weight volatile compounds such as CH_4, CO, H_2, and C_2H_2 were still in the gas-phase state. Although the increase in the temperature of pyrolysis led to the rise of specific surface area, pH_{pzc}, porosity, and pH of bio-char, it made the number of acid functional groups such as phenolic -OH and -COOH decline dramatically, resulting in the reduction in the adsorption ability of heavy metals in complexation (N. Ahmed et al., 2017). More noticeably, the extremely

high temperature of the pyrolysis process (over 900 °C) could lead to ash softening and melting, pore-clogging, and the number of pores reducing because of the merging of adjacent pores and pore extension (H. Li et al., 2020).

2.4.1.3 Hydrothermal

The hydrothermal process is considered another method for bio-char production from biomass, in which wet biomass is thermo-chemically converted into hydrochar. Water's characteristics changed dramatically at higher pressures and temperatures, and it acted as an organic solvent that facilitated reactions normally catalyzed by bases and acids as well as enhanced biomass degradation (Maniscalco et al., 2020). The fundamental merit of the hydrothermal process was the capability of transforming wet biomass into high-yielding carbonaceous solids with no need for an energy-intensive drying approach. Additionally, other benefits could be customizable surface functionalities, surface capabilities, high calorific value, conductive behavior, the presence of a natural binder, and other things (Sharma et al., 2019). Despite the unknown specific process of the hydrothermal treatment, all dehydration, condensation, hydrolysis, aromatization, and decarboxylation were expected. Biomass the hydrolysis process was decomposed into lignin and saccharides, besides, water was removed from biomass during the dehydration step by removing the hydroxyl group (Bhatia et al., 2020). Meanwhile, aromatization was caused by the removal of CO_2 during the decarboxylation.

In comparison with bio-chars produced during thermochemical technique with high temperatures, bio-chars attained in hydrothermal liquefaction could maintain crucial functional groups in the process of carbonization, thus allowing these groups to become more viable for various applications (V. Kumar & Dwivedi, 2021). However, some drawbacks of hydrothermal bio-char including thermal recalcitrance, limited surface area, declined porosity and less aromatic structures could be obstacles for further investigations (Rezania et al., 2020).

2.4.1.4 Torrefaction

Another emerging method to generate bio-char was torrefaction using a low heating rate, it was also known as mild pyrolysis (L. Liu et al., 2021). With the use of different breakdown processes, the oxygen, carbon dioxide, and moisture in the biomass could be eliminated by inert ambient air without oxygen under the temperature of 300 °C (Z. Chen et al., 2021).

2.5. Factors Affecting Biochar Production

The bio-char yield, as well as its physical-chemical features (e.g. carbon concentration, surface area, functional group, and pore size), were primarily determined by the conditions of pyrolysis and kinds of feedstock which were utilized in its manufacture(Martins et al., 2021). Furthermore, because of the volatiles released during the pyrolysis, these factors had a considerable effect on the structure of the final char. Indeed, the conditions of pyrolysis such as heat transfer rate residence time, and temperature strongly affected the bio-char characteristics and yields (Pandey et al., 2020).

The temperature of pyrolysis was considered a critical thermodynamic factor determining bio-char properties. In other words, this temperature parameter greatly influences the structure and characteristics of bio-char (Usman et al., 2019). Besides, pH, surface area, and ash concentration of bio-char made from biomass increased as temperature rose (Ho et al., 2012), while bio-char output declined (Yorgun and Yıldız, 2015). At low temperatures of pyrolysis, bio-chars created had cellulose and aliphatic-type structures, giving the substance a more diverse organic property. In a recent study (Shakya and Agarwal, 2019), they indicated that the increase in pyrolysis temperature resulted in increasing pore volume, pore diameter, and surface area.

The formation of multilayered carbon structures like honeycombs has demonstrated the dominance of aromatic content in bio-chars in the case of increased pyrolysis temperature. Unambiguously, progressive volatilization of organic matter during the pyrolysis process of biomass was thought to form deep channels with clear pores that appeared more prominently with an increase in pyrolysis temperature (Waqas et al., 2018). However, 550 °C was seen as the optimal pyrolysis temperature with the largest pore volume, pore diameter, and surface area. Indeed, the over-high pyrolysis temperature could release organic volatiles and displace the organic structure, resulting in the demolition of the porous structure. As increasing pyrolysis temperature to 650 °C. The destruction of bio-char structures with over-high pyrolysis temperature was indicated in previous publications (Tan et al., 2015).

The impacts of residence time are often connected with the temperature and heating rate of pyrolysis; according to (Zhang et al. 2015a), the yield of bio-char decreased when residence time increased with the temperature unchanged. When it comes to slow pyrolysis, the char yield could take advantage of longer residence time which improved the depolymerization of char

compounds (Park et al., 2008). Moreover, with a rise in residence time at a certain pyrolysis temperature, while the volatile matter concentration of biochar dropped, there was an increase in the fixed carbon content (Sun et al., 2017).

Additionally, another parameter that affected the biochar properties was the feedstock composition. Indeed, biomass rich in lignin could produce macroporous biochar with a pore size over 50 nm while the one rich in cellulose could primarily develop microporous bio-char that had a pore size of less than 2nm (Li et al., 2017). More importantly, micropores mainly took responsibility for the superior capacity of absorption as well as the high surface area (N. Ahmed et al., 2017).

The size of biomass particles was another crucial factor that affected the pyrolysis product distribution, the rates of mass transfer and heat as well as the secondary reaction degree in particles. The feedstock and pyrolysis process type in use determined the raw material's particle size. Particles with bigger diameters (over 1.8 mm) were discovered to get higher temperature gradients, which resulted in lower temperatures in the core compared to those on the particles' surfaces. As a result, the yields of char and liquid increased and yields of gas products and bio-based oil decreased at the same time (Aysu & Küçük, 2014).

2.6. Engineered and Modified Biochar

Although the research on bio-char employed to eliminate heavy metals was intensively studied, it could be observed the poor adsorption ability of conventional pristine bio-char. Whereas, it was hard to desorb heavy metals that were adsorbed by bio-char when the desorption process or post-treatment was not added after the adsorption behaviors of bio-char. This caused the bio-char with the absorption of heavy metals to become toxic wastes with no suitable treatment (Gong et al., 2021). In addition, the chemical compositions and physical structures of bio-char could be affected by environmental conditions such as substrate acidity, moisture, and temperature. Importantly, bio-char must be modified to improve its pore fraction and the specific surface area or to produce reactive functional groups before it can be employed as immobilization support. Chemical activation, physical activation as well as other activation approaches were considered the most common bio-char engineering approaches.

2.6.1. Physical Methods

Physical modification could improve bio-char attributes like volume, surface area, and pore structure. Furthermore, physical activation which involved the employment of physical agents (e.g. nitrogen, carbon dioxide, and steam) was able to rise chemical characteristics including hydrophobicity at the surface, functional groups, and polarity. Interestingly, in this inexpensive and simple technique of modification, chemicals were unnecessary (Leng et al., 2019).

2.6.2. Chemical Methods

The most often utilized method for activation was chemical activation (so-called wet oxidation). Chemical modification primarily involved metal salts modification, acid modification, oxidizing agent modification as well as alkaline modification. To obtain target features for engineering bio-char, acids (e.g·H_2O_2, H_2SO_4, H_3PO_4, HNO_3, and HCl), alkali (NaOH and KOH) along oxidizing reagents were employed in chemical engineering methods (Kołtowski et al., 2017). The employment of chemical agents like inorganic salts, bases, and acids to activate bio-char both changed the important physicochemical characteristics and created surface functional groups to boost the sorption capacity (Feng & Zhu, 2018).

Indeed, treatment with the use of oxidizing agents and acids helped increase the hydrophilicity of oxygen and functional groups that contain oxygen, whereas surface area along with porosity was reported to have varying effects (X. Yang et al., 2019). The reason why chemical alteration was more extensively used than a physical modification is that chemical modification possessed a few outstanding features as follows: (i) - Necessitated a short disposal time along with a low temperature for activation; (ii) - Activated biochar had a greater surface area; (iii) - Produced more activated bio-char; (iv) - Well-developed and evenly dispersed structure of microporous (Panwar & Pawar, 2022).

2.6.3. Other Methods

Bio-char composites aim to increase the sorption capacities of the metal ion. The goal of bio-char composites was to create novel functional groups on the surface of biochar, resulting in increased efficiency of metal ion absorption (Sizmur et al., 2017). Functional groups were commonly made by dipping raw biomass or bio-char generated in solutions of metal oxides or salts (such as chloride or nitrate) (He et al., 2018), and this involved numerous other pre- and post-processing stages. Possessing features like high surface areas and porous structures, biochar was ideal for

the deposition of metal particles which could generate a surface with a positive charge and, as a result, there would be a promotion in metal ion chemical sorption abilities (Wu et al., 2017).

In-situ activation or heterotopic doping could also enhance the bio-char quality. Biomass co-pyrolysis using dopants, activators, and other types of biomass resulted in the in-situ activation of bio-char. There also was an investigation on biomass co-pyrolysis with the presence of some activators or dopants like $FeCl_3$, KOH, $MgCl_2$, $KMnO_4$, $ZnCl_2$, urea, and Ca (OH) $_2$.

2.7. Factors Affecting Removal of Heavy Metals from Water Using Bio-Char

The adsorption of heavy metals by bio-char is not only related to the pore structure, surface cation exchange capacity, and number and type of functional groups in bio-char, but is also influenced by the dosage of bio-char, pH of water, water temperature, presence of other cations in water, initial concentration and type of heavy metals, and the bio-char aging process

2.7.1. Effect of Biochar Properties on Adsorption of Heavy Metals

Owing to the differences in the raw materials, pyrolysis temperatures used during bio-char preparation, as well as the modification processes, bio-char exhibits diversity in structure, pore distribution, elemental composition, pH, specific surface area, cation exchange capacity, surface functional groups, and other physical and chemical properties (Itoh et al., 2014).

The pore structure of bio-char, which determines the specific surface area, affects its adsorption capacity towards heavy metals. In general, the larger the specific surface area of biochar, the stronger its adsorption capacity. The high specific surface area and porosity of bio-char can provide more adsorption sites, and surface electricity affects the electrostatic interaction between bio-char and pollutants. Functional groups and mineral components are important structures for bio-char to combine with pollutants. Specific surface area and porosity are the main physical properties that affect the ability of bio-char to adsorb heavy metals.

2.7.2. Effect of Amount of Biochar Addition

The amount of biochar added is also a factor that causes differences in bio-char adsorption and is particularly significant in water polluted with mixed heavy metals. The amount of biochar added is generally positively correlated with the number of heavy metals adsorbed. However, when the amount of bio-char added reaches a certain value, the adsorption capacity reaches a stable level.

There exists a positive correlation between the amount of biochar added and heavy metal adsorption. However, when the amount of bio-char reaches a certain value, the adsorption capacity becomes stable. Therefore, the maximum removal rate can be obtained using the optimal dosage. A dosage of bio-char that is too high leads to reduced adsorption capacity. This may be due to the formation of tiny, agglomerated particles at high biochar concentrations, resulting in a decrease in the effective adsorption surface area (Dong et al., 2011).

2.7.3. Effect of Water Properties on Adsorption of Heavy Metals by Biochar

2.7.3.1. Water Temperature

Most of the studies have shown that the adsorption of heavy metal ions by biochar is an endothermic process. In other words, the adsorption of heavy metals by biochar is accompanied by the consumption of energy. An increase in temperature is beneficial for mutual adsorption (Y. Li et al., 2010). With the increase in temperature, the ion transfer rate is accelerated, which can not only accelerate the adsorption rate of biochar but also increase the adsorption capacity. Thus, ambient temperature also plays an important role in the adsorption behavior.

A higher temperature can provide more energy for the heavy metal ions to break through the diffusion layer on the biochar surface and enter the interior, which would increase the adsorption capacity. Temperature affects the adsorption rate by changing the intermolecular interaction and solubility. However, in the actual situation, the adsorption mostly occurs at room temperature, so additional heating or cooling of the solution should be avoided (Peng et al., 2017).

2.7.3.2 Effect of pH

Solution acidity or alkalinity is dependent on the concentration of H^+ in the polluted water, which relies on the type of water. The pH can affect the morphology of heavy metal ions as well as the surface charge distribution on bio-char, thereby affecting the adsorption rate and extent of heavy metal ions (Wan et al., 2020). At low pH values, the surface groups on the bio-char combine with H+, which reduces the negative charge, leading to reduced adsorption capacity for heavy metal cations. When the pH of the aqueous solution increases, the functional groups on the surface lose protons, thus leading to an increase in the negative charge and an increase in the adsorption capacity for heavy metal cations. In addition, alkaline precipitates of heavy metal cations are produced in alkaline solutions. Each heavy metal ion has a suitable pH range. pH values that are too low or too high are not conducive to the adsorption of heavy metal ions (Q. Chen, 2010).

2.7.3.3 Presence of Other Ions

In wastewater or natural water environments, in addition to heavy metal ions, a large number of other ions coexist in the water, and the concentrations of these ions also affect the adsorption of heavy metal ions. The presence of Na^{+}, K^{+}, Ca^{2+}, Mg^{2+}, Cl^{-}, NO^{3-}, and $SO4^{2-}$ ions in the solution can reduce the adsorption capacity of bio-char for heavy metal ions. With the increase in the ionic concentration, the number of heavy metals adsorbed by bio-char decreases. This is attributed to the presence of intrinsic ions in the solution, which not only hinders the release of ions from bio-char to water but also competes with heavy metal cations for adsorption on the bio-char surface. The intrinsic ions occupy the adsorption sites on the surface, affecting the removal efficiency of heavy metal ions (Mohan & Pittman, 2007).

2.7.3.4 Effect of Heavy Metal Ion Initial Concentration

Adsorption of heavy metals on bio-char is also dependent on the initial concentrations of the heavy metal ions. The higher the initial concentration of the heavy metal ions, the stronger the adsorption of heavy metal ions on bio-char. The key reason for this effect is that when the concentration of heavy metal ions is low, they only adsorb on the bio-char surface. When the heavy metal ion concentration increases, the internal structure of the heavy metal ions and bio-char starts playing a role, and the adsorption capacity increases (Mohan & Pittman, 2007).

2.7.3.5. Interactions between Heavy Metals in Polluted Water

Most of the polluted water samples contain multiple heavy metals, which experience both synergistic and competitive interactions among themselves. Different heavy metal ions coexisting in the solution compete with each other for adsorption sites. Compared with a single system, when a system contains two or more cations (or anions), the adsorption capacity or removal efficiency of the adsorbent is relatively reduced (Park et al., 2016). In binary systems or multi-component systems, the adsorption sites of carbon-based adsorbents have different affinities for heavy metal ions. The existence and difference of competitive adsorption behavior are determined by the charge and hydration radius of cations (Gan et al., 2015).

2.7.3.6 Effect of Ageing (Contact Time) Process on Adsorption of Heavy Metals by Bio-char

When bio-char is added to polluted water, the physical and chemical properties change over time, which is referred to as the aging process. Available results show that there is an increase in the number of oxygen-containing functional groups (such as hydroxyl and phenolic hydroxyl groups)

on the surface of bio-char after aging for a certain period, which can promote the adsorption of heavy metals (A. Kumar et al., 2018). On the other hand, a decrease in the specific surface area and pH leads to a decrease in the adsorption of heavy metals (H. Wang et al., 2017).

2.8. Adsorption Mechanism of Heavy Metals by Bio-Char

The adsorption activity of bio-char towards heavy metals is mainly dependent on its specific surface area, the number of surface-active functional groups, and cation exchange capacity (Gupta et al., 2020). Because many factors affect the adsorption of heavy metals by bio-char and the mechanism of action is complex, the dominant adsorption mechanism can vary even for a given heavy metal. Therefore, exploring the mechanism of heavy metal adsorption on bio-char can provide a theoretical understanding. According to existing research results, key adsorption mechanisms include physical adsorption, ion exchange, electrostatic adsorption, precipitation, complexation, and reduction. However, the adsorption of heavy metals by bio-char is not attributable to a single mechanism but rather involves a combination of multiple mechanisms (A. Zhang et al., 2020).

2.8.1. Physical Adsorption

Physical adsorption is caused by the van der Waals forces between molecules on the surface of bio-char and heavy metal ions. The heavy metal ions are either adsorbed on the surface or diffused into the pores of bio-char. Because physical adsorption is mainly caused by intermolecular forces, the adsorption affinity tends to be weak. Therefore, the adsorption process may be reversible. The main factors affecting the adsorption performance of bio-char are specific surface area and pore structure of the adsorption material, and biomass pyrolysis at high temperatures results in the formation of bio-char containing a large specific surface area and voids. This significantly increases the contact area between bio-char and heavy metal ions, improving the physical adsorption capability in water, fixation, and passivation of heavy metals in solution.

2.8.2. Ion Exchange and Surface Complexation

Ion exchange essentially involves the physical exchange of ions between the negatively charged surface groups on bio-char and positively charged heavy metal ions in solution and is caused by the Coulombic force between the surface groups and ions in solution. This is a nonspecific adsorption mechanism with low adsorption capacity

The oxygen-containing functional groups, such as hydroxyl, carbonyl, and carboxyl groups, on the surface of bio-char, can be used as adsorption sites for heavy metal ions. The solitary electron pairs on the oxygen atoms in these oxygen-containing functional groups form coordination bonds with the outer orbitals of heavy metal ions, forming stable complexes to immobilize the heavy metal ions (F. Huang et al., 2018).

2.8.3. Electrostatic Interactions and Redox Effect

Electrostatic interactions between the surface charges on bio-char and those on heavy metals are another mechanism involved in the remediation of heavy metals. The abundance of negative charges on the surface of bio-char enables the adsorption of positively charged heavy metal ions by electrostatic attraction (Uchimiya et al., 2012).Through electrostatic attraction, positively or negatively charged heavy metals can be fixed, as a result of which bio-char achieves an improved repair effect. Redox affects the chemical behavior, migration ability, and biological effectiveness of elements by changing their existing forms, mainly occurring in heavy metals with variable valence. The redox effect had a significant impact on the morphological distribution of heavy metals (Yuan et al., 2017).

2.9. Adsorption kinetics

The adsorption kinetic is one the most important issues for understanding both the mechanisms of adsorption and the assessment of influential factors on the reaction rate. Kinetics describes solute uptake rates and also defines the residence time of the adsorbate at the solid-liquid interface (Ahmadi et al., 2017).

2.10. Adsorption Equilibrium Isotherms

The adsorption equilibrium has always been explained by the isotherm equations such that their parameters indicate the surface characteristics and affinity of the adsorbent toward the adsorbate (Ahmadi et al., 2017)

Chapter Three

3. Methodology

3.1 Materials and Equipment

For the synthesis and characterization of WHBC and Activated-WHBC, and to analyze their physiochemical properties, different materials/equipment namely, analytical balance, water bath, pH meter, spatula, hot plate, sieve, measuring cylinder, beaker, grinder, temperature-controlled reactor/oven, magnetic stirrer, furnace, flask, vacuum pump, and mixer were used. Instruments such as Fourier transform infrared spectroscopy (FTIR), (scanning electron microscopy (SEM), surface area and pore size analyzer (BET), powder X-ray diffraction (XRD), and ultraviolet–visible (UV–visible) spectrophotometer were also used for analysis purposes.

3.1.1. Chemicals

Water hyacinth (raw material) was collected from the Oromia region in Lake Koka. All laboratory analyses and chemicals used in this experiment were prepared and carried out at the Adama Science and Technology University (ASTU), Adama, Ethiopia.

All chemicals used, including potassium hydroxide (KOH) for activation of biochar, hydrochloric acid (HCl)(35% purity), sodium hydroxide (NaOH)(99.8% purity), nitric acid (HNO_3)(69% purity), sulphuric acid (H_2SO_4)(98%purity), acetone(CH_3COCH_3)(99.5% purity), phenanthroline, hydroxyl amine (99% purity), ammonium acetate (99.54% purity) , and glacial acetic acid (99.5% purity) were of analytical grade. Distilled water and ammonium ferric sulfate ($(NH_4)_2Fe(SO_4)$) were used to prepare a stock solution of 200 mg/L of Fe (II). Various concentration solutions were prepared by appropriately diluting the stock solution. The initial pH level of solutions was adjusted using HCI and NaOH.

3.2. Collection of water hyacinth samples

In this study, the biomasses of water hyacinth were collected on Wednesday, November 29, 2024, at 4:10:46 AM from Lake Koka, Dungugi Bekele Kebele, Lume district, in East Showa administrative zone, Oromia regional state, Ethiopia as shown in the figure 3.1.

Figure 3. 1 : Water Hyacinth Infestation of Lake Koka in Dhungugi kebele

3.3 Sample preparation

The water hyacinth raw materials were manually collected and washed to avoid foreign matters such as stone, soil, and mud and then chopped to the appropriate size to fit the carbonizing kiln. The sample was cut separately into stem, root, and leaves with stainless steel, and these were dried on sheet paper to reduce extra moisture. For this study root part of the water hyacinth is taken for further experiment due to iron was highly accumulated in the root of the plant in comparison to the other parts of the water hyacinth plant (Belete et al., 2022). The samples of water hyacinth were dried in an oven (PRECISION, Model 6525) at 105 ^{o}C for 24 hours to a constant weight and size (1-2mm) and were stored or collected in a desiccator until needed.

3.3.1 Water hyacinth sample analysis

The dry biomass samples were characterized for proximate analysis, component analysis, and ultimate analysis, the most important characterization in biomass thermochemical conversion (Engineering et al., 2019). As follows:

3.3.1.1 Proximate analysis

A biomass sample's volatile matter, moisture, ash, and fixed carbon content are all estimated via proximate analysis. Each of these numbers is estimated using a method based on ASTM guidelines and literature (Márquez-Montesino et al., 2015). As follows:

3.3.1.2 Determination of moisture content

By precisely weighing 5 grams of powdered root water hyacinth using an electronic balance in a labeled, pre-weighed crucible, and then placing it in an oven to dry at 105 ^{o}C for three hours, the moisture content was calculated in triplicate. After drying, the crucible and dry sample were put in a desiccator to chill for 30 minutes before being weighed once more. Repeat the heating, cool, and weighing until a constant weight is achieved. The difference between the two subsequent weightings for the 5 g powdered water hyacinth sample was less than 2 mg. The moisture content was estimated as a percentage of weight loss (Akendo et al., 2008).

$$\% \text{ Moisture} = \frac{(W1-W2)*100}{W1} \qquad \text{(eq.1)}$$

Where W1=weigh before drying

W2 = weight after drying

3.3.1.3 Determination of volatile matter

By measuring 2 g of each sample in a crucible, covering it with a lid, and putting it in a muffle furnace at 800 °C for 8 minutes, the volatile matter of the root was measured in triplicate. The samples were then weighed after cooling in a desiccator. The volatile matter content was determined by dividing the percentage of weight loss by (Engineering et al., 2019):

$$\%\text{VM} = \frac{(W1-W2)*100}{W1} \qquad \text{(eq.2)}$$

Where VM = volatile matter

W_1= weight of sample before drying

W_2=weight of sample after drying

Three replicates were obtained and the results averaged

3.3.1.4 Determination of ash content

Weighing 2 g of the sample into a crucible, it was then heated at 600 ^{o}C for three hours in a muffle furnace to estimate the ash content in triplicate. Then the crucibles were taken out from the furnace and put into the desiccator to cool. The weight was measured after cooling to calculate the amount of ash (Engineering et al., 2019).

$$\% \text{ of ash} = \frac{(W2)*100}{w1} \qquad \text{(eq.3)}$$

Where W_1 = weight of the sample before drying

W_2= weight of sample after drying

Three replicate analyses were done and the results averaged

3.3.1.5. Determination of fixed carbon

According to the equation below, the percentage of fixed carbon was calculated by deducting the total of the percentages of volatile matter (PVM) and ash content (PAC) from 100:(Fallavena et al., 2014).

$$\text{Fixed Carbon} = 100\% - (\text{PVM} + \text{PVC}) \qquad \text{(eq.4)}$$

3.3.2. Component analysis

The following techniques were used to determine the concentrations of extractives, hemicellulose, cellulose, and lignin in water hyacinth samples (Márquez-Montesino et al., 2015).

3.3.2.1 Determination of extractives in the biomass (water hyacinth)

To quantify the amount of extractives in the biomass, solvent extraction was performed. 1 g of the dry biomass sample was mixed with 60 mL of acetone, and the temperature was maintained at 90 ^{o}C for two hours. The sample was then dried in an oven (105–110 ^{o}C) until it reached a consistent weight. The amount of the extractives is shown by the weight difference before and after the extraction (Engineering et al., 2019). Three replicates were obtained and the results were averaged.

3.2.2.2 Determination of hemicellulose in the biomass (water hyacinth)

1 g of dried biomass devoid of extractives was mixed with 150 mL of sodium hydroxide (NaOH) solution at a concentration of 0.5 mol/L for 3.5 hours at 80 ^{o}C to measure the amount of hemicellulose. The sample was next rinsed with deionized (DI) water until no more Na^{+} was found, which is shown by the solution's pH value nearing 7, and then it was dried to a consistent weight. The amount of hemicellulose is what causes the sample weight to fluctuate between before and after this treatment. The outcomes of three duplicate analyses were averaged (Engineering et al., 2019).

3.2.2.3 Determination of lignin in the biomass (water hyacinth)

Lignin was determined based on its insolubility in 98 % H_2SO_4. For each gram of the sample (extractive-free dried biomass), 30 mL of 98% sulfuric acid was added to calculate the amount of lignin. The sample was kept at 25 ^{o}C for 24 hours before being cooked at 100 ^{o}C for one hour. The mixture was filtered, the residue was washed until there was no longer any sulfate ion present in the filtrate, and it was then dried to a consistent weight. The lignin content is calculated based on the weight of the residue. The results were averaged over three replicate analyses (Engineering et al., 2019).

3.2.2.4 Determination of cellulose in the biomass (water hyacinth)

By assuming that extractives, hemicellulose, lignin, ash, and cellulose are the only components of the total biomass, the cellulose content (%w/w) was estimated by difference(Lin et al., 2010).

3.4 Biochar Preparation

A crucible cup in a muffle furnace was used for the production of the water hyacinth biochar. During the production process, the crucible cup with a lid was wrapped with tin foil. The grounded sample water hyacinth was tightly placed in a porcelain capsule and then Briefly, around 5g for each raw water hyacinth was compacted in a 250 mL ceramic pot enveloped with aluminum foil to create artificial environment to reduce direct exposure with air and calcinated in a muffle furnace model SX-2.5-12 under oxygen-limited conditions at various temperatures (i.e., 300, 400, 500, 600 °C, and 700 °C) for (1 and 2hr) (H. M. Yang et al., 2017).Water hyacinth-derived biochar (WHBC) was left to cool down at room temperature and conserved in a desiccator. Finally, the samples were stored in a sealed plastic container. The WHC samples obtained at calcination temperatures of 300, 400, 500, 600, and 700^{o}C were labeled as

WHBC300, WHBC400, WHBC500, WHBC600, and WHBC700 respectively. Preliminary duplicate adsorption tests were conducted using these all adsorbents to select the WHBC with the highest adsorption efficiency for further WHBC activation.

3.5. Activation of Biochar (KOH)

Compared to WH, the KOH-activated WH possessed more microporous structures and larger BET, which was due to the following processes. KOH was selected as the activating agent of choice because it is known to produce materials with good performance, high yields, high adsorption capacity, and well-defined pores as well as a high specific surface area under low activation temperatures (H. M. Yang et al., 2017). A mixture of KOH and biochar in the mass ratio of 25:75, 50:50 and75:25 was applied with 100 mL of distilled water in a 250-mL beaker placed on a hot plate and stirred for 2 hr. at 90 °C for complete mixing And it should be cooled for 2 hr. to form strong bond then washed by distilled water until the neutral pH was obtained and to remove any impurity .The mixture was then oven-dried at 110 °C for 24 h, and grinded and sieved through a 0.15 mm mesh to obtain uniform material. The final materials were kept in pre-cleaned plastic containers as WHABC for activated water hyacinth biochar.

3.6 Biochar Characterization

Different characterization methods were used to examine the properties of the WHBC, KOH-AC-BCH before and after adsorption. All the measurements in this study were performed in duplicate to ensure the quality and repeatability of the work.

Biochar yield was calculated as the ratio between BC and the dry weight of water hyacinth biomass.

FTIR analysis: The surface functional groups of activated water hyacinth-derived biochar samples before and after adsorption were examined with a Fourier-transform infrared spectroscopy (FT-IR). The attenuated total reflectance FTIR with model name FTIR-6600 type A and serial number A013861790 in the range of 4000 to 500 cm^{-1} was used. The sample for the FTIR analysis was prepared by weighting the amounts of sample, 1 gm, and Potassium Bromide (KBr) powder, 100 gm into an agate mortar. The FTIR pattern is plotted within the FTIR machine by generating the transmittance peaks (%) as the Y-axis versus wavenumber (cm-1) as the X-axis.

XRD analysis: The crystallographic structure in water hyacith and modified water hyacinth-derived biochar before and after adsorption were identified by X-ray diffraction (XRD) analysis model Shimadzu XRD-7000 x-ray diffractometer using cu-kα radiation. The measurement condition for each test includes voltage = 40.0 (kV), current = 30.0 (mA), and scan range from 10.00 to 70.00 with 0.02 step size.

SEM analysis: A scanning electron microscope (JCM-6000PLUS Bench Top SEM, JEOL, Japan) was employed to visualize the surface morphology and structure of the activated water hyacinth biochar before and after adsorption. The procedure of analysis includes a 30 mg specimen mounted on a metal stub using a sticky carbon tape, which increases conductivity. The clip holds the sample securely and the clip does not obscure any area that you intend to image. The specimen must be electrically grounded to the sample holder to minimize specimen charging. Specimen exchange, evacuation, and automatic adjustment of the image were carried out for photographing and finally, the image was saved.

BET analysis: The textural properties of water hyacinth biochar and activated water hyacinth (surface area, pore volume, and average pore diameter) were determined by the N2-BET method using a surface area and porosimetry analyzer (SA-9600 Series, Horiba Instruments, Inc.) at 200^{o}C degassing temperature for 2 hr. in the presence of nitrogen gas.

UV/vis spectrophotometer analysis: The iron concentration (initial and final), was determined using the UV–Vis spectrophotometer (Hach DR6000TM, LPV441.99.00002, USA).

pH of point of zero charge (pH_{PZC}) measurement: The pH drift method was applied to measure pH_{PZC} values. This method is less time-consuming, and the results are perfect than the ones obtained from other applied methods such as titrations. Accordingly, solutions of 50 ml of iron solution prepared in different Erlenmeyer flasks were adjusted to pH values of 1.0 to 12.0 using 0.1 M NaOH and 0.1 M HCl. Then, 0.5g of KOH-AC-WHL was added to an Erlenmeyer flask containing iron solution and shaken for 24 hours. The final pH of the samples was measured and plotted against the initial pH (Pashai Gatabi et al., 2016). The intersection point of the resulting curve with the line passing its origin gives pH_{PZC}. The pH of the solutions was monitored on a pH meter.

3.7 Preparation of calibration chart

Stock solution containing iron is prepared using 500-ml standard volumetric flask, and using this solution different ppm concentrations of 100 ppm, 90 ppm, 80 ppm, 70 ppm, 60 ppm and 50 ppm were prepared by diluting the standard solution using 500-ml standard volumetric flask. Placing the different ppm solutions in the cuvette observed the reading for absorbance in the photoelectric colorimeter (Nallakukkala et al., 2021). The concentration is then plotted on a graph against absorbance as shown in Fig.3.8 thereby generating a calibration curve. Final concentration is calculated by the Beer-lamberts law

$$A = \varepsilon lc \quad \text{Where:} \qquad \text{(eq. 4)}$$

ε = molar absorption coefficient which is equal with slope of calibration curve ($M^{-1}cm^{-1}$)

l = optical path length A = absorbance c = molar concentration

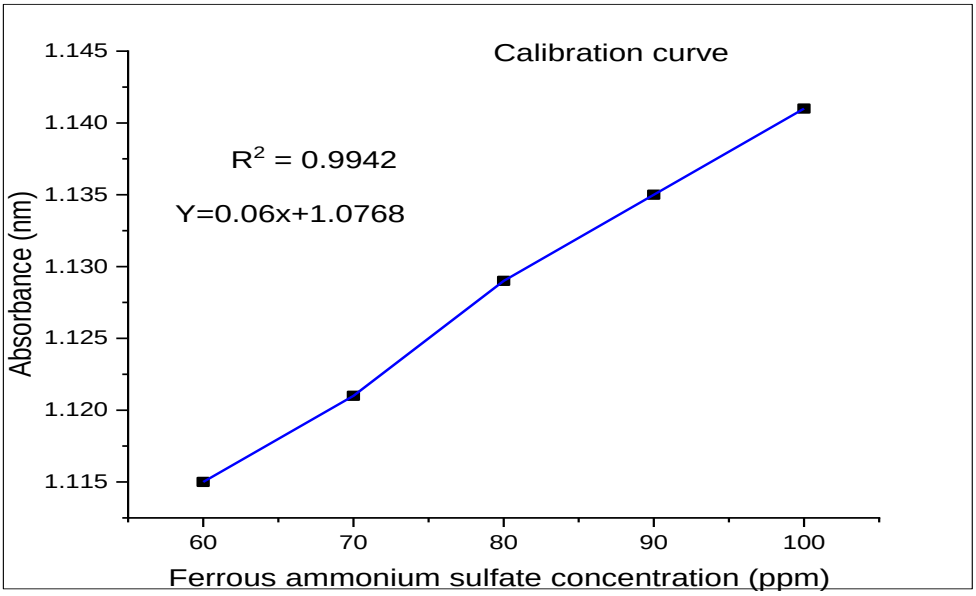

Figure 3. 2: Calibration curve of iron

3.8 Biochar Adsorption Experiments

Adsorption experiments were conducted to determine the potential of the biochars to adsorb Fe(II) from aqueous solutions. The period between fabrication and use of biochar in adsorption experiments is within three days.

To determine the optimum conditions for Fe(II) removal by adsorbents from aqueous solution, batch adsorption experiments were carried out in 500 mL conical flasks using a magnetic stirrer. The effects of contact time (10–120 min) (30, 60, 90, and 120 min), initial Fe(II) concentration (50–100 ppm)(50, 60, 70, 80, 90, and 100ppm), adsorbent dosage (0.5–2 g/L)(0.5, 1, 1.5 and 2g), and initial pH (4–10)(4, 5, 6, 7, 8, 9, and 10) on adsorption performance were investigated. The effect of contact time on Fe(II) removal was studied using 50 mL of 10 mg/L solutions of Fe(II) agitated with 0.1 g/L of the adsorbent for different contact times (10–120 min). The effect of pH was investigated using 160 mL of 10 mg/L solutions of Fe(II) adjusted to initial pH 4–10 and agitated with 0.1 g/L of the adsorbent for 30 min. The effect of the adsorbent dose was studied by agitating 160 mL of 10 mg/L solution of Fe(II) containing different doses of adsorbent (0.1–2.0 g/L) for 30 min. The effect of initial iron concentration was studied by agitating a 50 mL solution containing different concentrations of Fe(II) (50–100mg/L) for 30 min with 0.1 g/L of adsorbent.

After agitation, samples were collected and the solids were removed by filtration through a 0.45 µm pore size filter paper. The final metal concentration in the filtrate and the initial concentration were determined using an atomic absorption spectrometer (Varian AA240FS, Australia). The adsorption capacity qe (mg/g) and removal efficiency of Fe(II) at equilibrium were calculated as follows:

$$qe\left(\frac{mg}{g}\right) = (Co - Ce)V/W \qquad \text{(eq.5)}$$

$$\text{Removal efficiency } (\,)\% \;=\; 100 \text{ x } (\text{Co} - \text{Ce})/\text{Co} \qquad \text{(eq.6)}$$

Where qe (mg/g) is the adsorption capacity, Co and Ce (mg/L) are the initial and equilibrium iron concentration, respectively, V (L) is the solution volume, and w (g) is the adsorbent mass.

3.9. Adsorption Isotherm

To simulate the adsorption isotherms of Fe(II), the Langmuir (Eq.7) and Freundlich isotherms (Eq.8) were used in fitting the experimental data. The Langmuir model assumes that monolayer

adsorption occurs on homogeneous surfaces with no interactions among adsorbed ions. The Langmuir model is often used to describe adsorption capabilities and reflects the absorption equilibrium process. The Freundlich isotherm model assumes that multilayer adsorption occurs on heterogeneous surfaces and that the adsorption amount increases infinitely with increasing concentration. Moreover, the Freundlich isotherm model provides information on chemisorption on heterogeneous surfaces.

$$\text{Langmuir: } \frac{Ce}{qe} = \frac{1}{KLqmax} + \frac{ce}{qmax} \qquad \text{(eq.7)}$$

$$\text{Freundlich: } \ln(kf) + \frac{1}{n}\ln(ce) \qquad \text{(eq.8)}$$

where q_e (mg g^{-1}) is the equilibrium Fe(II) adsorption capacity in the solution, q_{max} (mg g^{-1}) is the maximum capacity, Ce (mg L^{-1}) is the equilibrium concentration of Fe(II), n is the Freundlich constant related to adsorption intensity, and K_L (L mg^{-1}) and K_F (mg L^{-1} /n L^{-1} /n g^{-1}) represent the adsorption constants for the Langmuir and Freundlich models, respectively.

3.10. Adsorption Kinetic

Kinetic investigation into sorption was performed to describe the adsorption mechanism and assess the efficiency of Fe(II) adsorption. Pseudo models were used to simulate the adsorption kinetics of Fe(II) concerning the biochars. First-order (Eq.9) and second-order (Eq.10) equations describe the kinetics of solid solution systems based on mononuclear and binuclear adsorption, respectively, concerning sorbent capacity. The pseudo-second-order kinetic model assumes that adsorption capacity is proportional to the number of active sites occupied by the adsorbent.

$$\text{First-order equation: } \frac{dqt}{dt} = k1(qe - qt) \qquad \text{(eq.9)}$$

$$\text{Second-order equation: } \frac{dqt}{dt} = k2(qe - qt)^2 \qquad \text{(eq.10)}$$

Where qt and qe are the amounts of Fe(II) adsorbed at time t and equilibrium, respectively (mg kg^{-1}), and k_1 and k_2 are the first-order and second-order apparent adsorption rate constants (h^{-1} and kg mg^{-1} h^{-1}), respectively.

3.11. Adsorption of Fe (II) onto (AC-WHBC) in Real Wastewater

To apply the laboratory experimental result to the practical real-world application, the investigation was carried out by taking real water, which has 150mg /L amount of total iron from steal factory wastewater. The laboratory report indicates the real water contains a high concentration of Cr, Mn, and Fe, which have the value of 0.23 mg/L, 0.61 mg/L, and 150 mg/L respectively. The adsorption process is conducted at optimum parameters, including pH = 6, contact time =90 min, initial concentration of iron = 50mg/L and adsorbent dose = 1g/L.

3.12. Desorption and Regeneration Experiments

The regeneration studies were conducted according to reference (Quintelas et al., 2009). In brief, 50 mg/L Fe(II) ions concentration, 1.0 g/L adsorbent dosage, the solution pH 6.0, was agitated for 90 min at room temperature. The KOH-AC-WHL, in the recovered solution, was filled with deionized water and shaken for 180 min. Then, the sorbent was filtered, and the equilibrium concentration of desorbed ions in an aqueous solution was measured. The process was repeated four times.

Chapter Four

4. Result and Discussion

4.1 Wastewater Characterization

The WHO advises drinking water to contain the following amounts of inorganic pollutants 0.3 mg/ L (Fe, regulated for aesthetic reasons) (WHO 2011). The real wastewater used in the present study had the following initial pollutant concentrations of iron, nickel, copper and lead is 30, 3, 2 and 0.01mg/L respectively. These concentrations were far above the WHO thresholds.

4.2 Characterization of raw water hyacinth biomass

4.2.1 Proximate analysis

Figure 4.1 displays the outcomes of the proximate analysis performed on the water hyacinth samples. Fig 4.1 indicates that the content of volatile matter (VM) on WH is predominant with the value of 65.13 (wt. %). A low value of VM indicates that biomass is hard to burn or will affect its low reactivity, and vice versa. Meaning that the higher the VM, the more susceptible the biomass to burn and the higher its reactivity. Therefore, the high VM content of WH infers that this biomass is reactive during the combustion process (Sukarni et al., 2014).

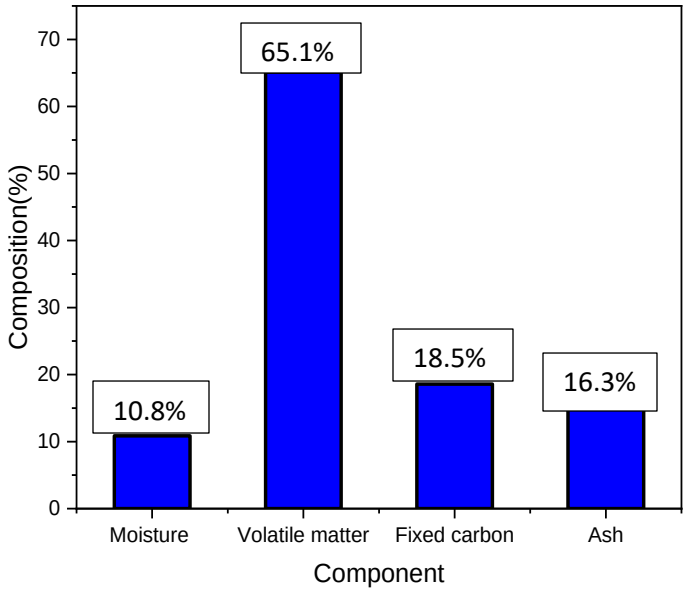

Figure 4. 1: Proximate Analysis of Water Hyacinth (dry basis wt. %)

Ash (A) becomes the second largest content with a value of 16.3 (wt. %). This high ash content is influenced by the inorganic elements which are non-flammable parts of biomass (Obernberger et al., 2006). These elements are derived from mineral fractions of biomass origin. The ash content of biomass fuel is tightly related to accuracy choice of combustion technology and gas cleaning method. In the combustion system, the residual handling method and overall operating cost are strongly determined by the ash fuel content. Thus, fuel with the minuscule content of ash is highly desirable.

It was discovered that 18.57 weight percent of fixed carbon, which is obtained entirely from the lignin component of biomass material, is transformed into biochar and other carbonaceous compounds in thermochemical conversion processes.

Last but not least, WH has a 10.87 (wt. %) moisture content. In comparison to its volatile content, this figure is quite small. It is seen favorably since less energy is required for the evaporation process during thermal conversion the lower the water content.

4.2.2 Component analysis of water hyacinth

Figure 4.2 displays the findings of the chemical composition study of water hyacinth. By understanding the component so, that we explore the way to convert in to value added product. According to the findings, cellulose, hemicellulose, and lignin make up the majority of the aquatic plant. Hemicellulose has the highest composition of 38.2 wt %, followed by cellulose at 25.10 wt %. Lignin concentration is 6 wt %, the least. The results are comparable to what was obtained in previous studies, which had cellulose (18.20 – 26.10 wt), hemicellulose (26.80 – 48.70 wt %), lignin (3.50 – 6.30 wt %), and extractives (13.30 – 18.00 wt %) (Nigan, 2002; Luo et al., 2011).

Hemicellulose is the material that can be pyrolyzed the simplest, followed by cellulose, and lignin is the most challenging. Cellulose and hemicellulose are the primary components of biomass that are transformed into bio-oil and bio-gas, whereas lignin makes up the solid residue, or bio-char (Asadullah et al., 2007; Jahirul et al., 2012; Fukuda, 2015). The main components of biomass that are converted into bio-oil and bio-gas are cellulose and hemicellulose, whereas lignin makes up the solid residue or biochar.

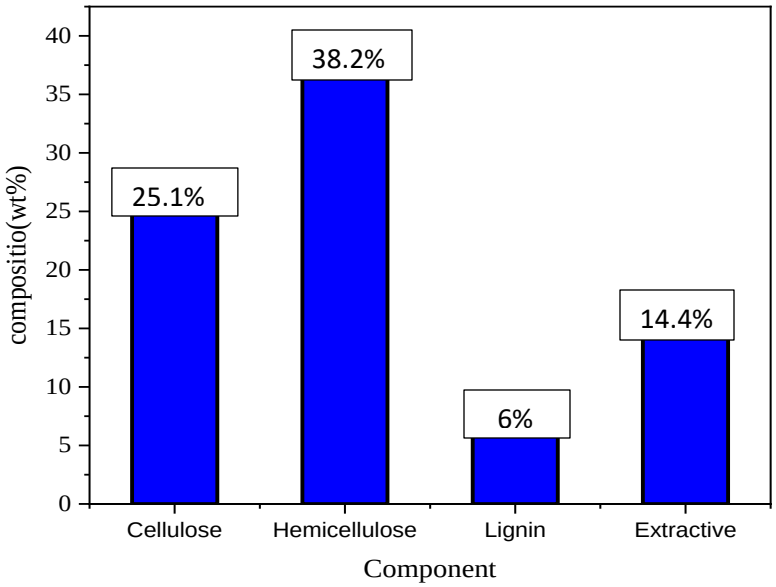

Figure 4. 2: Component Analysis of Water Hyacinth (dry basis wt. %)

4.3 Effects of Calcination Temperature on Biochar Yield

Table 4.1 shows the yield amount, in percentages, of the water hyacinth obtained at various calcination temperatures. The yield of the material decreased with increasing calcination temperature. The calcination temperature negatively but differentially affected the biochar yield. Usually, as the calcination temperature increases, there is the removal of the volatile matter from the biomass, causing the biochar yield to decrease (Yadav and Jagadevan 2019) and there is a sintering and shrinkage of biochar which become denser and more compacted.

Table 4. 1 Biochar yields obtained for water hyacinth at different calcination temperatures

Biochar	BC300	BC400	BC500	BC600	BC700
Yield (%)	50	42	34.675	25	23

4.4. Optimum Conditions for Synthesis of Adsorbents

The removal efficiency of water hyacinth char highly depends on calcination temperature and calcination time, the process of calcination has several purposes to water hyacinth char. Firstly, it activates the material by removing impurities and volatiles, resulting in increased surface area and pore volume. This activation enhances the adsorption capacity and efficiency of water

hyacinth char calcination and eliminates organic matter present in the water hyacinth char through high-temperature combustion(K. Yadav & Jagadevan, 2020). Generally, the calcination temperature and the duration of calcination affect the extent of activation and the degree of structural modifications.

4.4.1. Effect of the Calcination Temperature

During this experiment, the calcination time, initial iron concentration, contact time, adsorbent dosage, and solution pH were kept constant at 1 hr, 50 mg/L, 30min, 0.5 g/L, and 7 respectively. As shown in Figure 4.3, the iron removal efficiency increased from 58 to 85.2 % as the calcination temperature raised from 300 to 500 ^{o}C.

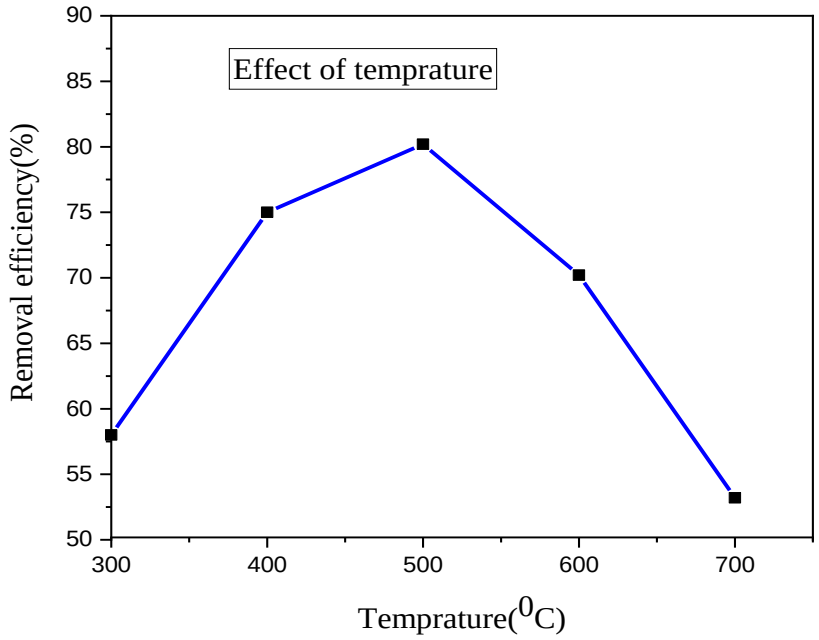

Figure 4. 3: Optimum calcination temperature

This was due to low temperatures, below 500 °C caused more organic matter originally in the water hyacinth biochar to be added to the treated water due to inadequate removal of organic matter in the bone structure (Alkurdi et al., 2019).

However, with further increased temperatures from 600 and 700 ^{o}C, the iron removal efficiency decreased from 70.2 to 53.2 %. According to Rojas-Mayorga et al., (2015), at lower calcination temperatures an increase in temperature might help to increase pore volume and surface area on

the adsorbent and the reverse is expected as shown in figure 4.3. And may results in the loss of certain functional group which are essential for adsorption.

4.4.2. Effect of calcination Time

This experiment was employed at an initial iron concentration of 50 mg/L, a calcination temperature of 500 ºC, a contact time of 30min, an adsorbent dosage of 0.5 g/L, and a pH of 7. While keeping these constant conditions, different calcination times of 0.5, 1, 2, and 3were varied and tested.

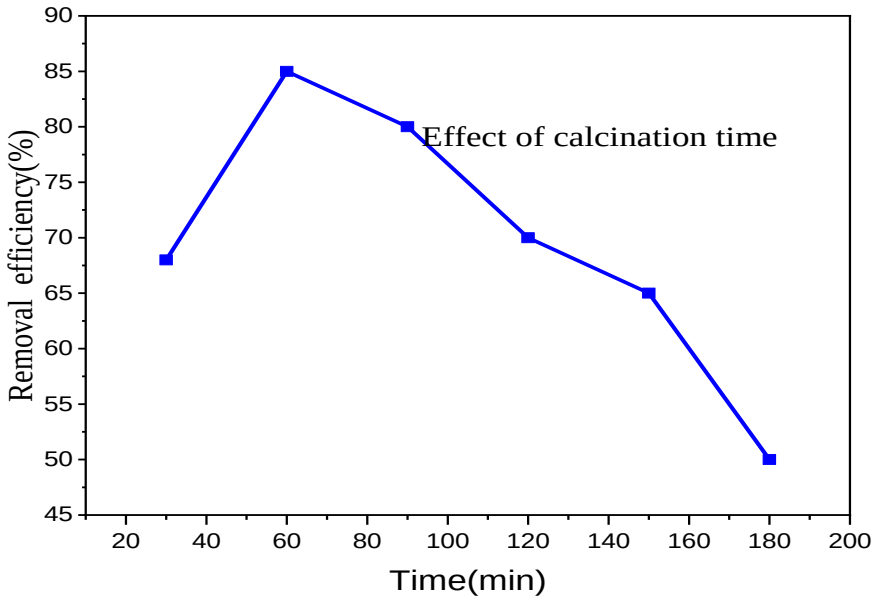

Figure 4. 4: Effect of calcination time

As depicted in Figure 4.4, it was observed that iron removal efficiency increased at a time raised from 0.5hr to 1hr, whereas an increase in the pyrolysis time beyond 1 hr. shown gradually decreased the iron removal efficiency due to loss of functional group (Nallakukkala et al., 2021).

4.4.3 Effect of mixing ratio of KOH and water hyacinth biochar

The effects of KOH and water hyacinth biochar mass ratios on the adsorption performance was explored in Fig. 4.5. As observed, the Fe(II) uptake increased from 60% to 83% as the KOH: biochar mass proportions elevated from 25:75 to 75:25. So that as the mass of activater (KOH) increases the removal efficiency also increases thus providing powerful evidence for the

adsorption improvement of original biochar by KOH activation but we are taking the biochar as a precursor material for the research so that the best mass ratio was 50:50 as shown in the graph from the angle of cost effectiveness of the process may increase the cost of production due to the higher amount of activating agent is required.

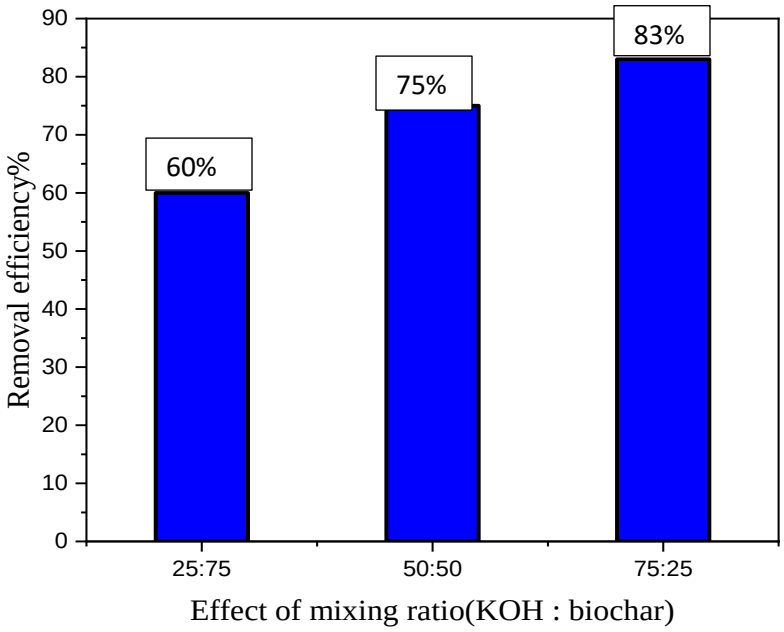

Figure 4.5: Effect of mixing ratio

4.5 Adsorbents characterization

4.5.1 Brunauer-Emmett-Teller (BET) Analysis

The values of Brunauer–Emmett–Teller (BET) surface area, pore radius, and pore volume of the adsorbents are shown in Table 4.2. These values reveal that the adsorbents have favorable adsorption properties. KOH-WHBC has the highest BET surface area (528 m^2 /g) and pore volume (2.1 cm^3 /g) which indicates that KOH-WHBC has the highest capacity to remove iron ions compared to other adsorbents. The pore volume of the adsorbents corresponded to the same increasing trend as the surface area as follow: KOH-WHBC > WHBC. Therefore, the modified activated carbons with potassium hydroxide (KOH-WHBC)s have high adsorption properties compared to other adsorbents.

Table 4. 2: BET surface property result for WHBC and KOH-WHBC composite

Sample	Surface area(m^2/g)	Total pore volume (cm^3/g)	Pore radius (Ao)
WHBC	400.249	1.587	0.145
KOH- WHBC	528	2.1	1.324

4.5.2 Scanning Electron Microscope (SEM) Analysis

The surface images of the WHB, KOH-WHBC before and after (a, b and c) were carried out by using SEM. The SEM micrographs of WHB are shown in Fig. 4.5. The micrographs show that the WHB has an inhomogeneous, rough surface. In addition, its surface contains many pores that vary in size, shape, and depth; this observation is consistent with other WHB prepared previously (Masto et al., 2013).

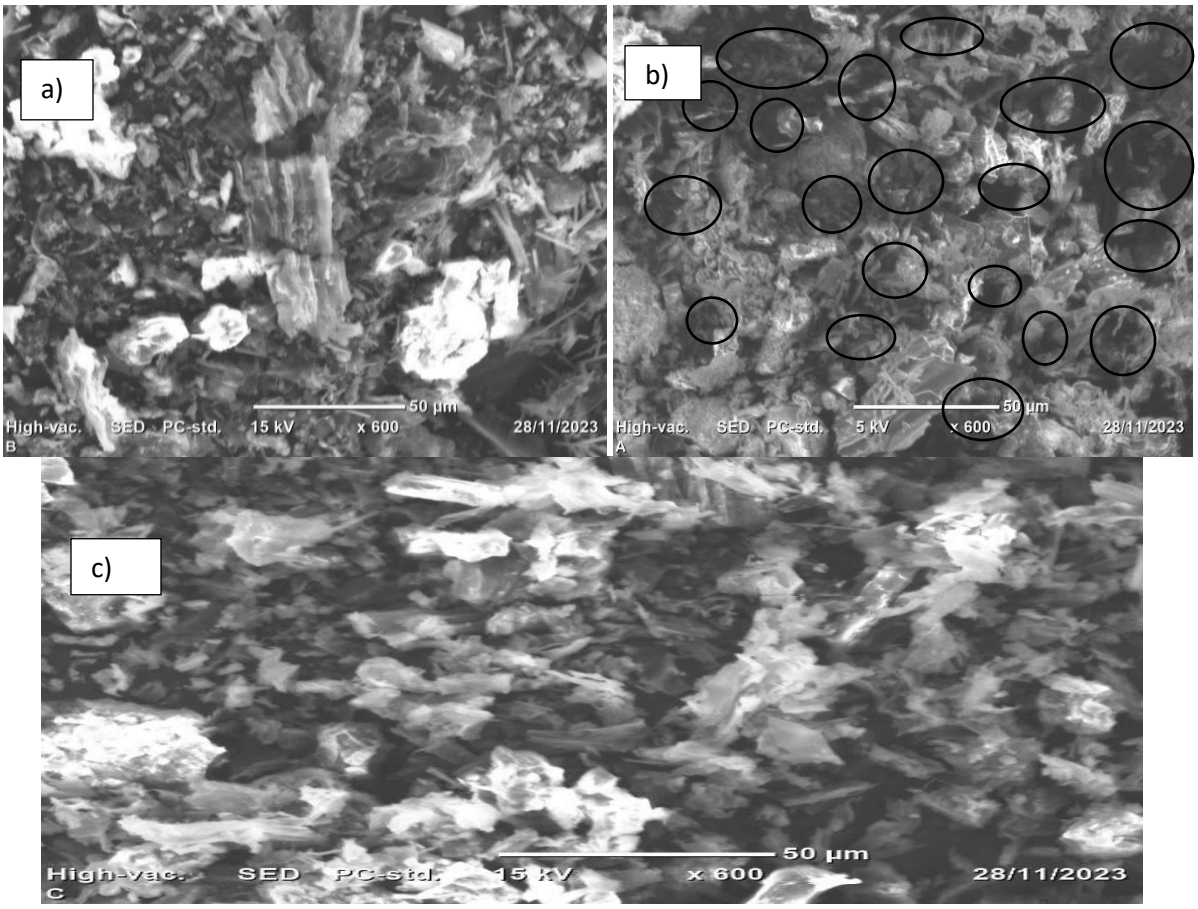

Figure 4. 5 : SEM images of a) Water hyacinth BC b) KOH-Water hyacinth BC before adsorption c) KOH-Water hyacinth BC after adsorption

When the WH biomass is calcinated, the volatile substances released from it result in the formation of micropores on its surface, while the volatiles, which were trapped inside the biomass, expand the microstructure. Consequently, WHB becomes a porous material with a high surface area (Z. Liu et al., 2015).Figure 4.5a) shows water hyacinth biochar wich was produced at a temperature and time of 500 ^{0}C and 1hr respectively. WHB in the figure forms needle like structure with less porosity and high agglomeration were observed for SEM image. Figure 4.5 b) shows activated water hyacinth wich was produced by with 1:1 ratio of adsorbent and KOH before adsorbtion process. KOH-WHBC is less agglomerated with better dispersion and pore site observed. This change were observed due to activation of biochar, resulting in the collapse and shrinkage of the material. This can lead to a reduction in particle size. In addition, it may result in formation of new pore sites. The interconnected porosity makes it suitable for adsorption application. As shown in Fig. 4.5.b, the external surfaces of the activated carbons have considerable numbers of pores, which are of different sizes and shapes. The surfaces of KOH-WHBC (b) are rougher and features a higher porous structure than water hyacinth biochar and raised its adsorption capacity. The modification process is effective in forming well-developed pores on the adsorbents surfaces, leading to KOH-WHBC with larger surface areas and better porous structure (mesoporous). Nearly all heterogeneous types of pore structure were also distributed on the modified adsorbents surfaces. Fig. 4.5 c) shows the SEM images activated water hyacinth after adsorption it become again agglomerate and dense due to KOH-WHB loads iron(II).

4.5.3 Fourier Transform Infrared Spectroscopy (FTIR) Analysis

Fig. 4.6 represents the FTIR analysis of the biochar, activated and Fe(II) loaded biochar dictating a fluctuation of the peak intensity within 500-4000cm^{-1}. The FTIR spectra of the biochars (WHBC and KOH-WHBC) are shown in Fig 4.6. The band at 3,437 cm^{-1} represented the stretching vibrations of the OH groups, which could be attributed to the adsorbed water on the biochar. The asymmetric (2,927 cm^{-1}) and symmetric (2,854 cm^{-1}) C– H stretching bands were associated with aliphatic functional groups and were observed in WHBC but not in KOH-WHBC, thus indicating a decreased non-polar aliphatic fraction. The bands around 1,636 cm^{-1} were attributed to the aromatic C = O and C = C. The C = O functional groups showed very high coordination with the heavy metals. The bands at around 1,317 cm^{-1} were associated with the phenolic -OH or aromatic CO- stretching vibrations. In short, the functional groups observed on

the biochars included CH, OH, C = O, and CO, all of which may have contributed to the Fe sorption. On the basis of these results, we can deduce that the good sorption properties of the adsorbent toward Fe can be attributed to the presence of the functional groups in the adsorbent.

The shift (600 cm^{-1}) indicates the alteration of frequency in the functional groups of the biochar due to the adsorption of iron. A significant band shift in the region of 500–1500 cm^{-1} is due to hydroxyl groups of phenols present on the adsorbent surface (Saranya et al., 2017). The appearance of the peak aroun 500 cm^{-1} in KOH-WHBC is due to the adsorption iron by Eichhornia crassipes biochar. As shown in Figure 4.6. This means that the groups were participating in the adsorption to a certain extent to produce new functional groups as a result of the complexation Fe(II) ions with the main functional groups which are in agreement with the reference (W. Chen et al., 2018).

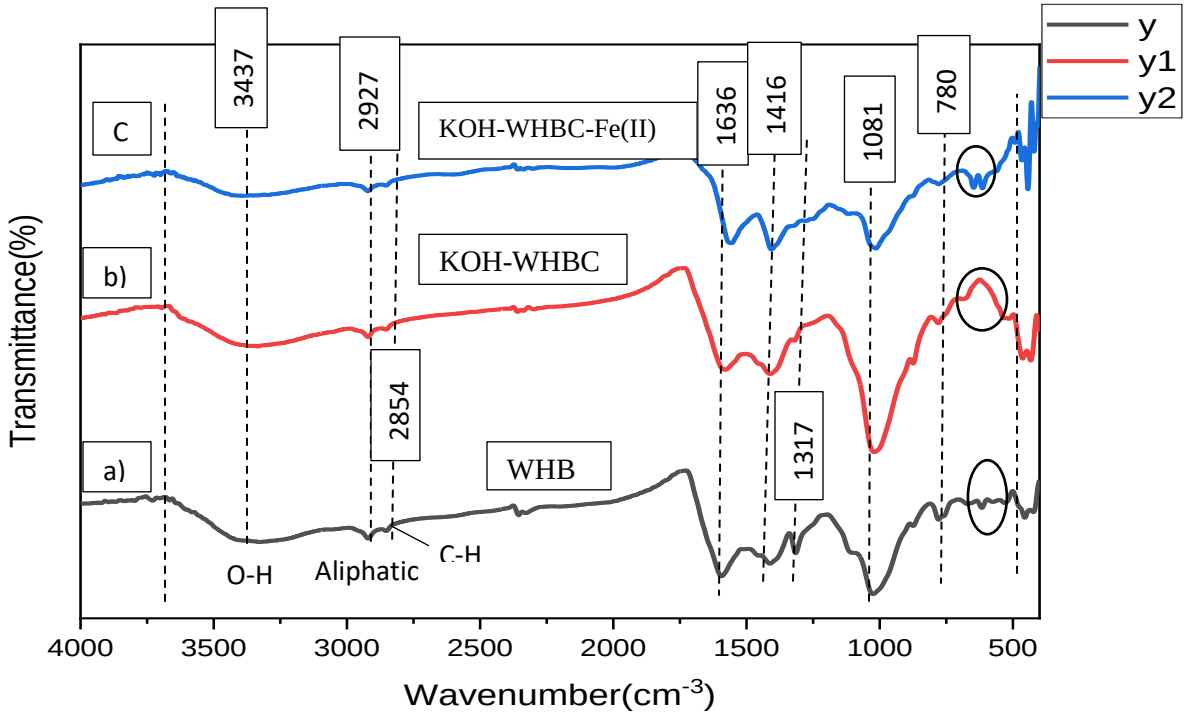

Figure 4. 6. FT-IR spectra of a) WHB, b) KOH-AC-WHB, and c) KOH-AC-WHB-Fe(II)

As shown in the figure 4.6b) The KOH-AC-WHL presents peak around 3470, 2927, 2847, 1739, 1640, and 1090 cm^{-1} which was attributed to vibration of O–H, sp3 C-H, sp2 C-H, C=O, C=C, and C-O functional groups, respectively. The FT-IR spectrum for KOH-AC-WHL-Fe(II)

figure4.6c) shows the shift, disappearance, and decrease in the intensity of the peaks due to the interaction of Fe(II) ions with hydroxyl and carboxyl functional groups. This means that the groups were participating in the adsorption to a certain extent to produce new functional groups as a result of complexation Fe(II) ions with the main functional groups which is in agreement with reference (Ley 25.632, 2002).

4.5.4 X- Ray Diffraction (XRD) Analysis

The XRD curves of RWHB and KOH-WHB are shown in Fig. 4.7. The XRD patterns of RWHB and KOH-WHB were analyzed. Powder XRD (Shimadzu XRD-7000 X-ray diffractometer using Cu-Kα radiation) was used to determine sample crystallinity throughout this work. The XRD patterns confirmed that the diffraction peaks correspond to the crystal structure and phase purity of synthesized material. The diffraction peak of WHB consists of a poorly crystalline phase compared to the KOH-WHB as shown in the figure 4.7 (a). A decrease in the peak width and a considerable increase in the peak height were observed with KOH-ₓWHB. The two curves seem to have nearly the same distinct peaks, indicating the presence of the same crystalline phase, with much more elevation in the area from 9 to 50^0 in the WHBC than that of the KOH-WHB. Two broad peaks were appeared at the 2 theta value of around 9^0 and 32^0 for raw WHBC. These might related to crystallinity in lattice spacing of cellulose. On the other hand, the KOH-WHB XRD curve (Fig. 4.7b) showed that the peaks at the same angles disappeared and appearance of small pick. The peaks 2 theta value of (15^0,19^0,24^0,28^0,38^0,39^0,50^0,and 62^0) show new appearance of peak and angle shifting due to the activation of biochar by KOH and there is also a 2 theta value (35^0 and 45^0) dis appearance of paek due some reaction(Shaaban et al., 2013).

Figure 4.7 b)shows the XRD plot of KOH activated WHBC according to the observed peaks, KO_3 and $K_2CO_3{\cdot}(1.5)H_2O$ were identified in the product of chemical activation (peaks at 2θ = 32.5°, 39.8°, and 41.9° for KO_3 and peaks at 2θ = 15°, 29.8°, 30°, 32.5°, 32.7°, and 41.5° for $K_2CO_3 \cdot[1.5H_2O]$). More study is required to specify the other possible potassium compounds in the product.Figure 4.7a) showes five sharp distinct peaks at 2 theta values of the WHBC curve appeared at approximately 9^0,29^0, 30^0, 32^0, 35^0 and 45^0 · In this study, carbon in the water hyacinth-derived biochar have possessed an amorphous carbon structure, natural organic matter-like structure, and condensed graphitic structure (crystallite) during the calcination process at a temperature (500 °C) (W. Chen et al., 2018). Meanwhile, crystals also formed in the ash of

inorganic minerals with a relatively high content. According to analysis in the Search-Match software, the main crystal structure is potassium salt (KCl). Moreover, the weak diffraction peak at 2θ=29.1 depicts the stacking of the monatomic carbon layer in crystallites, which indicates that the organic crystalline compounds in water hyacinth have been carbonized into graphitized crystallite carbon with finer grains.

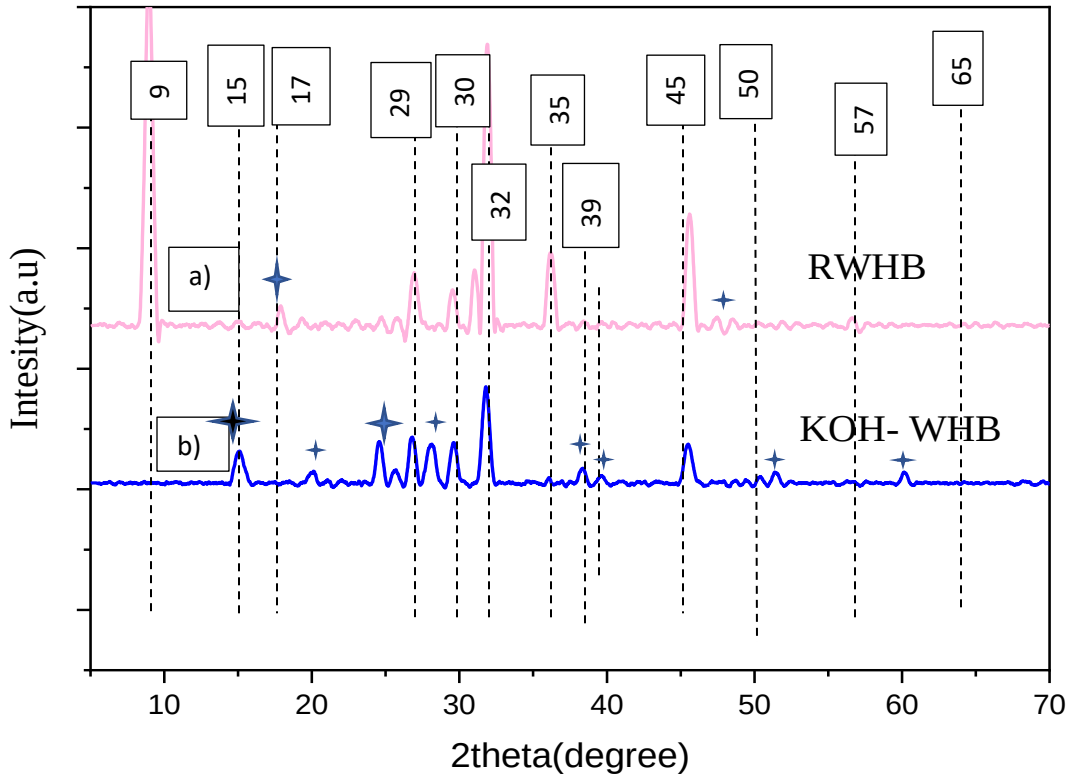

Figure 4. 7: XRD patterns of the water hyacinth-derived biochar

4.6 Point of zero charge (pH_{PZC})

KOH-AC-WHBC's pHPZC was discovered to be 3.4, as seen in the figure below the point at which the surface is electrically neutral. At pH < 3.4, Fe(II) ions are prevented from adhering to the surface of KOH-AC-WHBC by electrostatic repulsion. The negatively charged accessible active sites on the KOH-AC-WHBC progressively increased with increasing pH, creating a strong electrostatic attraction that favored the adsorption of Fe(II) ions. Above the pH of 3.4 the

surface tends to carry a net of negative charge due to adsorption of (OH-) and below the pH of 3.4 the surface tends to carry a net of hydrogen ion (H+)

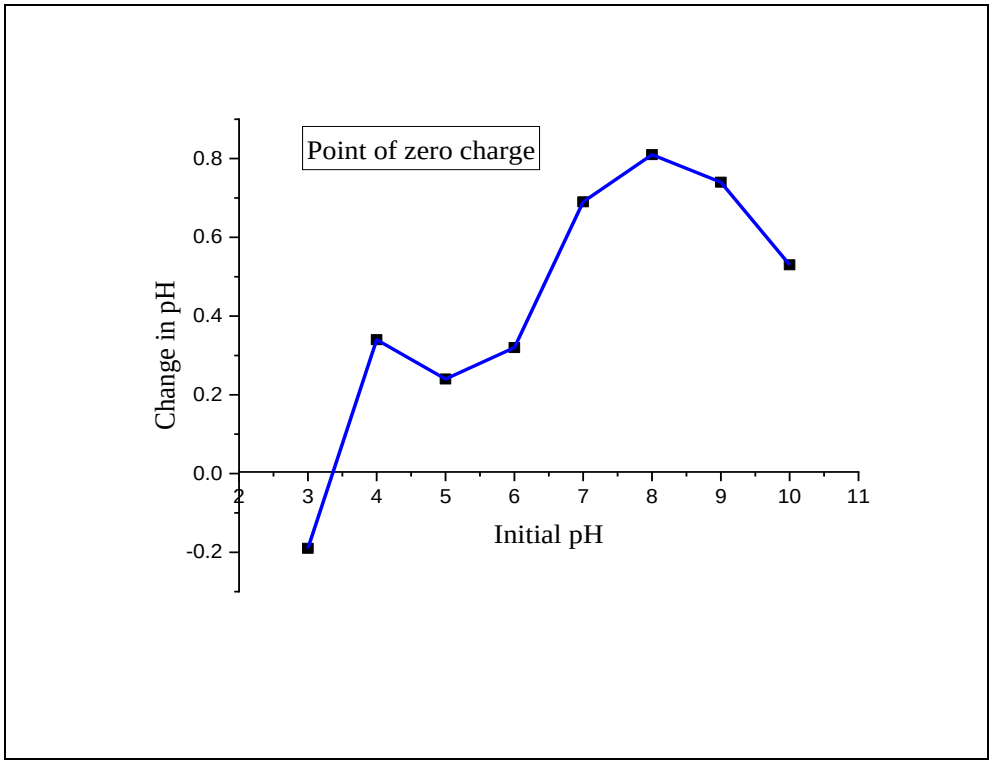

Figure 4. 8: Determination of point of zero charge on KOH-WHBC

4.7 Factors Affecting Iron Adsorption

4.7.1 Effect of pH of the solution

At low pH levels, in the range of 1 to 5, the concentration of H^+ ions is more comparable to that of heavy metal ions; additionally, the prepared activated adsorbent has a greater affinity for H^+ ions than for iron metal ions. Hydrogen ions also tend to compete with iron metal ions for the adsorbent adsorption sites. As a result, less adsorption is seen at lower pH values, which may be related to the presence and greater mobility of H^+ ions. Similar to this, at high pH levels in the range of 8 to 14, the adsorbent surface's negative charge density increases, increasing the attraction between the metal ion and the adsorbent as shown in figure 4.9. The produced activated adsorbent exhibits a greater affinity for the OH^- ion in comparison to the heavy metal ion.

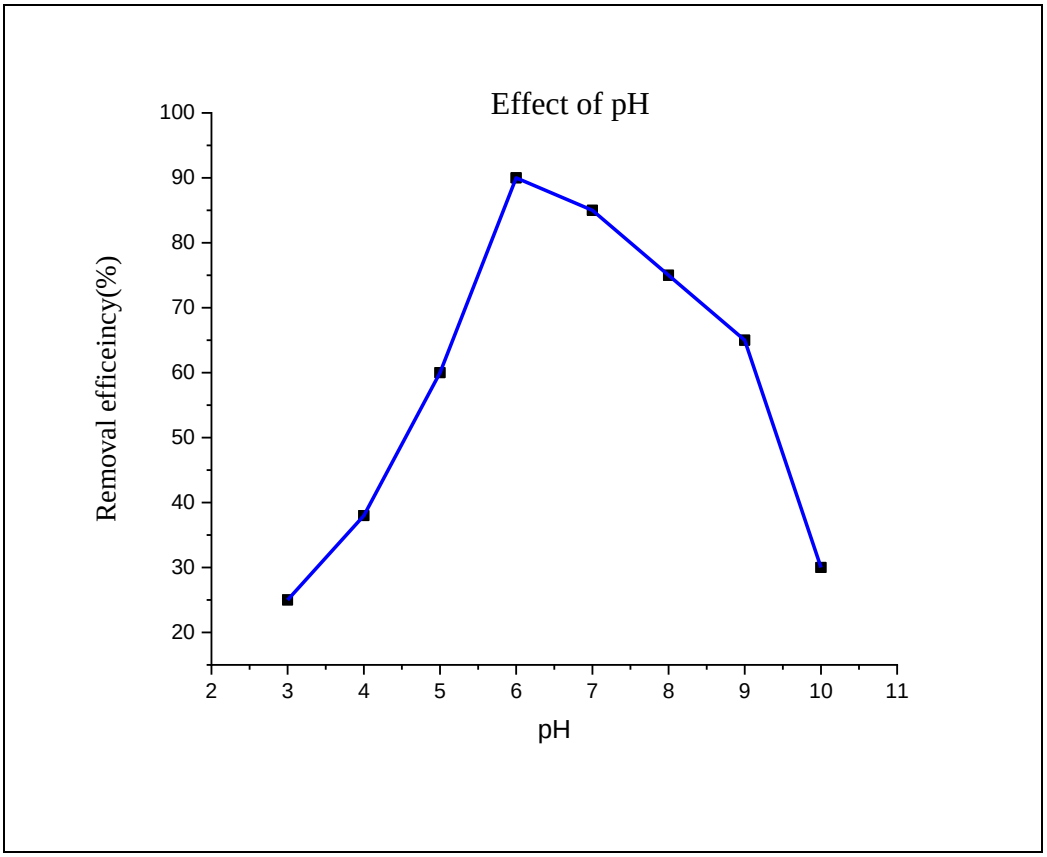

Figure 4. 9: Effect of pH on iron metal ion removal

Fewer adsorbent active sites were left behind when the pH rose from 3.0 to 6.0, making more negatively charged active sites available for electrostatic interaction and facilitating the adsorption of the positively charged iron metal ions. One possible explanation for the modest decrease in adsorption at pH 7 is the production of soluble hydroxyl complexes, such as $Fe(OH)_2$. This suggests that adsorption reduces at high pH values. However, based on the graph, the ideal pH level was determined to be 6, as this was the maximum adsorption and removal efficiency found there.

4.7.2 Influence of Initial Ion Concentration

Fig. 4.10 illustrates the impact of adsorbent dosage on Fe(II) removal efficiency at pH 6. The adsorbent dosage is 0.5g/L, and the incubation period is fixed at 0.5 hours. As illustrated in Fig.4. 10, small initial ion concentration have lower removal efficiency due to mass transfer limitation and equilibrium may not balance which shifts towards to desorption and an increase in the initial ion concentration causes a decrease in the iron removal effectiveness against an iron-containing

aqueous mixture. This is because at lower concentrations, sufficient adsorption sites are available, allowing the Fe^{2+} ions to come into contact with those sites. Adsorption efficiency is reduced at higher concentrations because chemically activated carbon adsorption sites remain soaked. Based on the graph, the ideal starting ion concentration is 50 ppm.

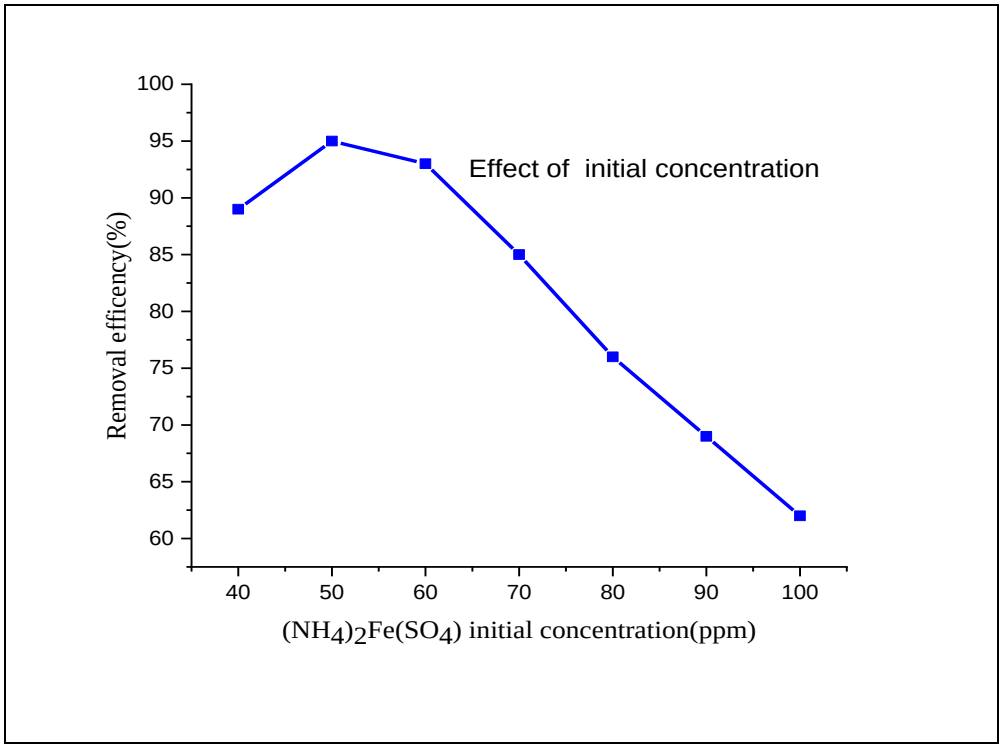

Figure 4. 10: Effect of initial ion concentration on iron metal ion removal

4.7.4 Effect of adsorbent dosage

The effect of adsorbent dosage on percent removal and adsorption capacity was shown in Figure 4.11. Increasing KOH-AC-WHBC dosage increases the percent removal while decreasing the adsorption capacity, an effect also reported by others (Y. Huang et al., 2014). The increased adsorbent dose provides additional active sites leading to increased percent removal. But, at high adsorbent concentrations, the percent removal reaches a maximum constant value. This is due to the agglomeration of the adsorbent which decreases the unoccupied adsorption active sites and the effective surface area. The initial concentration and volume of Fe(II) ions are constant; the number of ions contacted and adsorbed by the adsorbent per unit mass decreases with the

increase in the adsorbent dose, and the active sites of the adsorbents are not saturated. Hence, with the increase in the adsorbent dose, the adsorption capacity of Fe(II) gradually decreases, and similar results are reported in reference(Lei et al., 2019) . So that from the figure 4.11 up to 1g/L of adsorbent dosage the removal efficiency increases and after that it becomes constant due to all site become occupied.

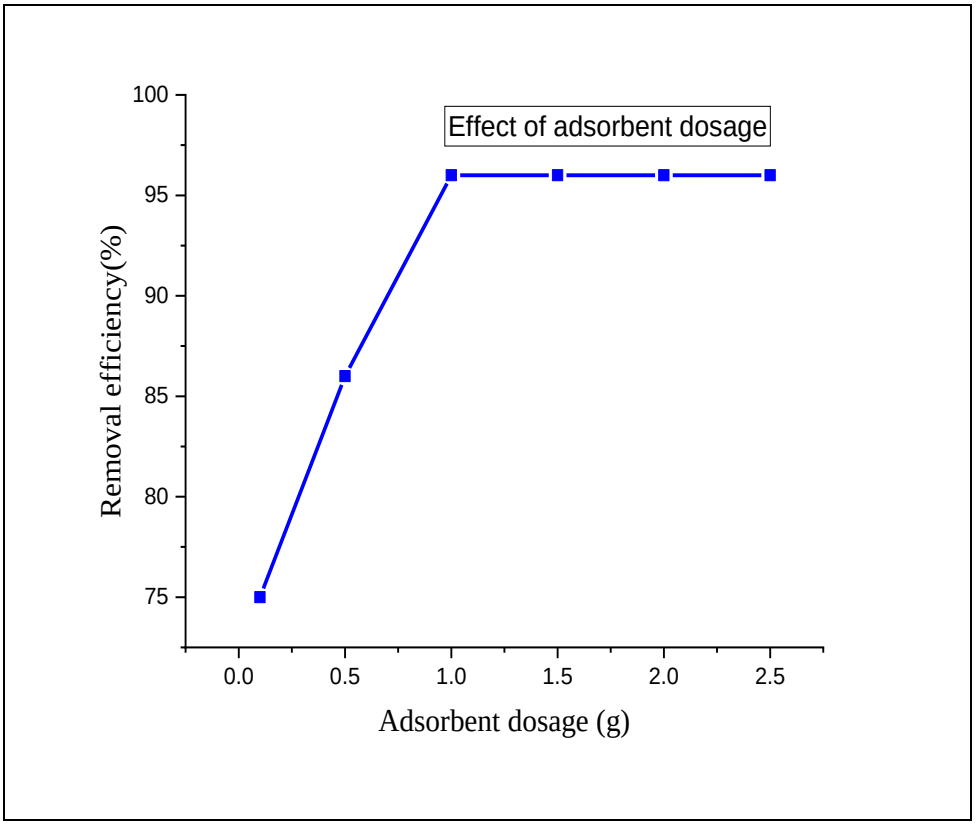

Figure 4. 11: Effect of biochar dosage on iron metal ion removal

4.7.3 Effect of Contact Time

As shown in figure 4.12 early in the sorption phase, there was a noticeable quick increase in the adsorption capacity, which thereafter began to diminish progressively after around 90 minutes. This may have to do with the adsorbent's early stage having an extraordinarily high volume and pores open for ion uptake or adsorption. Fe(II) ion adsorption proceeded quickly for the first sixty minutes, and then steadily approached equilibrium after ninety minutes. Fe(II) ions had an removal efficiency of 99.3%, and maximum sorption was reached after 90 minutes. Furthermore, a further increase in contact time had no discernible effect on the metal ion's

adsorption capacity, most likely as a result of the adsorbent surface becoming saturated with Fe(II) ions, which is consistent with reference (Yahya et al., 2020).

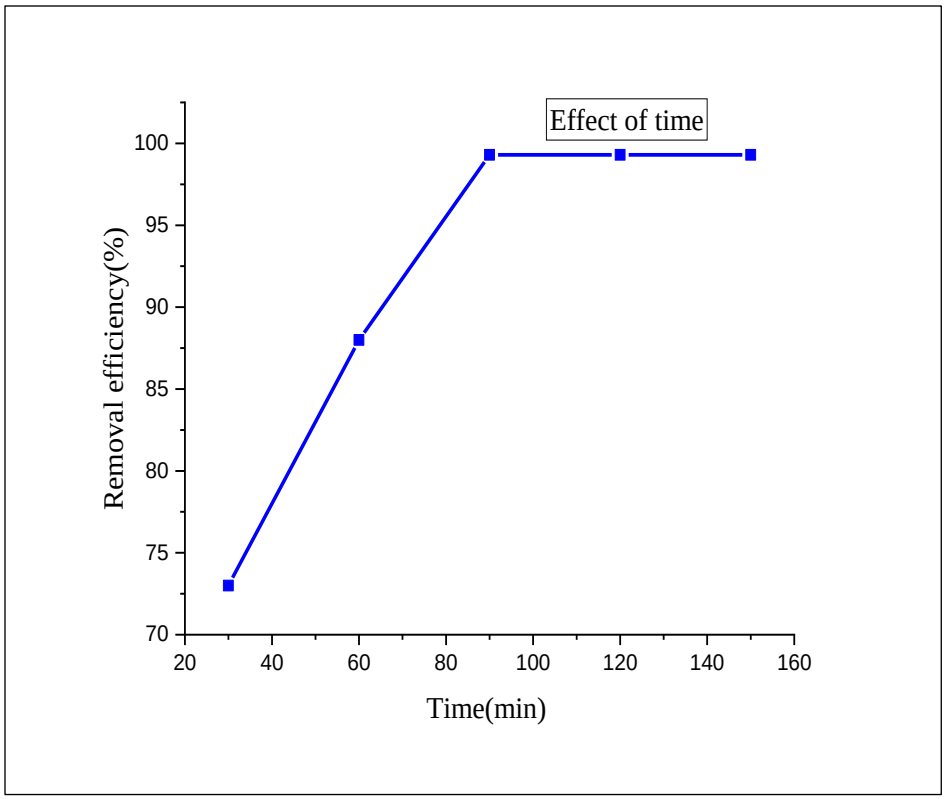

Fig 4.12. Effect of time on iron metal removal

The adsorption of Fe(II) ions was fast for up to 60 min due to early stage of the adsorbent have high volume and pores open for adsorption and thereafter they gradually reached equilibrium at 90 min. Maximum sorption was obtained at 90 min, with Fe(II) ions showing an adsorption capacity of 65.5 mg/g. Moreover, a further increase in contact time had no significant influence on the adsorption capacity of the metal ion, probably due to the saturation of the adsorbent surface with Fe(II) ions which is in agreement with reference (Yahya et al., 2020). Therefore, the optimum contact time was chosen as 90 min for the process and further investigation.

4.8 Adsorption isotherm and kinetics

4.8.1 Adsorption isotherm

In order to gain better understanding on the possible Fe(II) sorption processes by the water hyacinth-derived biochar, the empirical Langmuir and Freundlich models were utilized to fit the abovementioned adsorption data. The Langmuir isotherm model (Fig. 8.13a) assumes that the surface of the adsorbent possesses the same active adsorption sites and the adsorption process takes place in a single molecular layer (Febrianto et al., 2009).The Freundlich isotherm model (Fig. 8.13b) assumes that the adsorption enthalpy is multiphasely distributed on the surface of adsorbent and enhances with the increasing adsorbent surface coverage. The Freundlich adsorption isotherm has the highest R^2 value 0.97 respectively. This result indicated the occurrence of multilayer adsorption on a heterogeneous surface(Kong et al., 2017). While, the Langmuir model fits well for the adsorption of Fe(II) on KOH-WHB adsorbent (R^2 = 0.986), which indicates monolayer sorption with a finite number of identical sites (Y. N. Wang et al., 2016).

4.8.2 Langmuir and freundlich adsorption isotherm

This defines quantifiable information on the development of a monolayer adsorbate on the adsorbent external layer. Langmuir adsorption isotherm signifies the equilibrium dispersal of metal among the solid liquid streams, and it is effective for monolayer adsorption comprising to limited amount of alike positions. This isotherm considers even adsorption on the surface of adsorbate. From the graph 4.13a variables are calculated from the slope and intercept of Langmuir graph of ce /qe vs Ce where K_L is found 0.0021. The freundlich technique is implemented to define the adsorption features for the heterogeneous system.

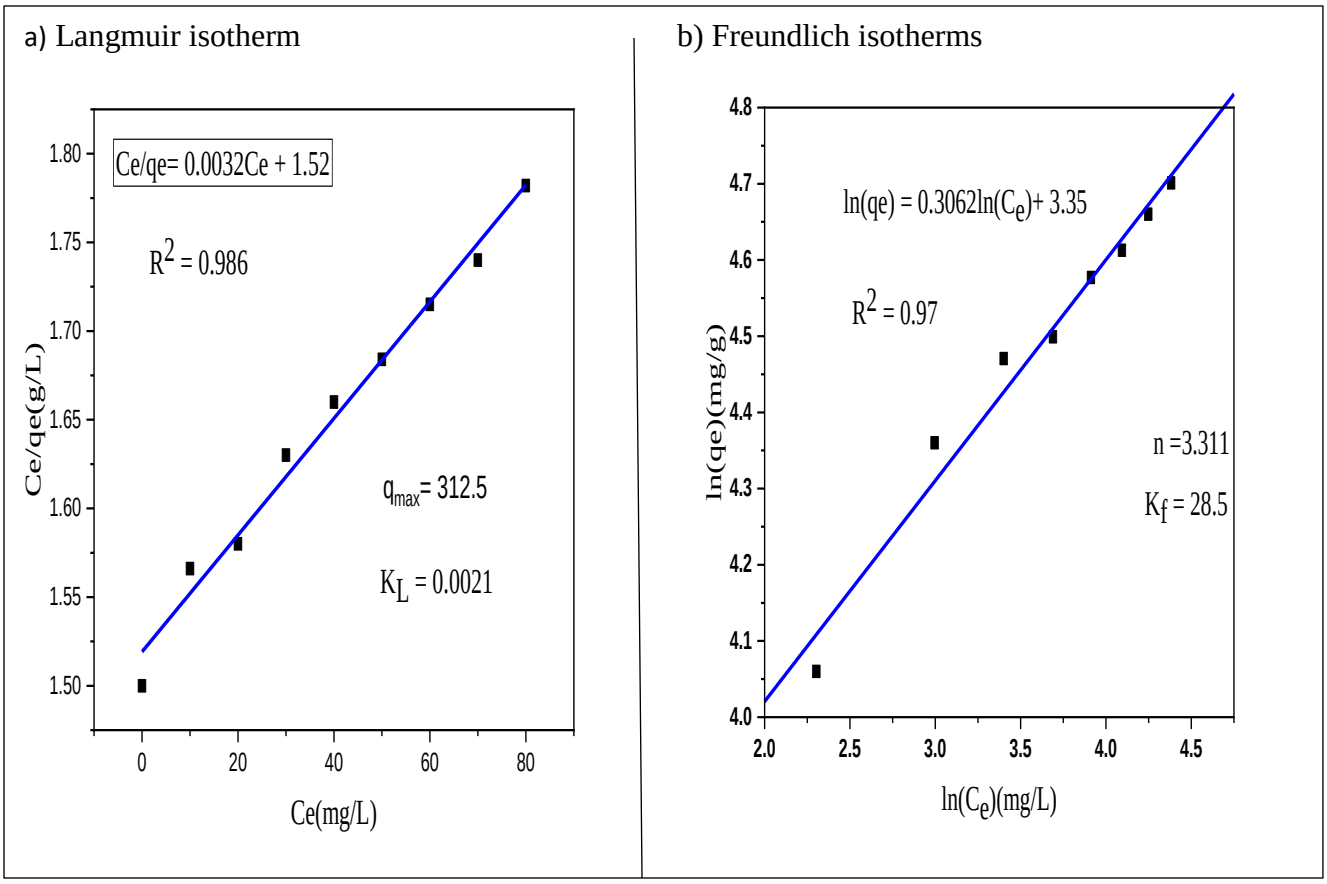

Figure 4. 12: Linear model fitting of a) Langmuir and b) Freundlich isotherm

The constant K_f is adsorption capacity indicator, and 1 n is a function of the adsorption strength. If n=1, the barrier among the two phases remains concentration independent and when the value of 1 n < 1, it designates normal adsorption. As there is rise in temperature, the constants k and n vary to show that adsorbed amount increases gradually and in order to saturate the surface higher pressures are required. The least-squares technique and linearly transformed equations can be used in order to relate adsorption information where 1 n signifies heterogeneity. If n is between 1 and 10, then it designates a promising adsorption phenomenon. From Fig. 4.12 it is found that K_f is 28.5.32 and n is 3.311.The experimental data of Fe(II) adsorption were regressively simulated with the two models and the results are displayed in Fig. 4.12,

Table 4.3: Model adequacy measures

Isotherm	parameters	Value
Langmuir	q_{max} (mg/g)	312.5
	K_L (L/mg)	0.0021
	R^2	0.986
Freundlich	n	3.311
	1/n	0.302
	k_f (mg/g)(1/mg)$^{1/n}$	28.5
	R^2	0.97

The parameters obtained from the linear fitting of Langmuir and Freundlich models provide important information on the affinity of the adsorbent, the sorption mechanisms, and the surface properties of the adsorbent. The Langmuir model gave the most accurate estimations R^2 =0.986 indicating that, a homogenous adsorption rate, with equal adsorbent affinity, with single-layer adsorption (M. Li et al., 2019). Maximum adsorption capacities obtained from the Langmuir model were 312.5 mg/g

4.8.3 Adsorption kinetics

The iron metal acceptance rate and equilibrium time on activated carbon are determined by the adsorption kinetics. Adsorbate kinetics is still crucial when determining the best operating conditions for a batch system. The kinetic parameters provide strong support for the process modeling and help estimate the rate of adsorption. Thus, kinetics is used to assess the effects of initial ion concentration, contact time, and adsorbent dosage. Different kinetic rate equations, such as pseudo-first-order and second-order models, are used to investigate the adsorption kinetics.

Table 4.3: Kinetics model parameters for Pseudo-first-order and Pseudo-second-order

Kinetics	parameters	Value
Pseudo-First Order	q_e (mg/g)	21.13
	K_1 (min^{-1})	0.00639
	R^2	0.712
Pseudo-Second Order	q_e (mg/g)	67.84
	K_2 (g/mg.min)	0.00264
	R^2	0.998

The kinetics of adsorption is analyzed by means of various kinetic rate equations such as pseudo-first-order and second-order model. The first-order rate constant k1 is accomplished from slope of the graph drawn between ln ($q_e - q_t$) vs time, as shown in Fig. 4.13. Table 4.3 data were obtained from Fig. 4.13.Second-order rate constant obtained from graph of t/qt versus t. The pseudo-second order kinetic equation is implemented by means of drawing graph between t/qt versus t, and the present kinetics resulted in higher values of regression correlation coefficient of R^2=0.998 as shown in Table 4.3.

The obtained experimental values suggest that the adsorption of iron metal ion on the chemically activated carbon satisfied the pseudo-second order kinetics, representing the suitability to adsorption phenomena. This factor indicated that adsorption of iron exhibits the second-order mechanism, demonstrating that chemical adsorption is the rate-limiting step among the metal and chemically activated water hyacinth carbon.

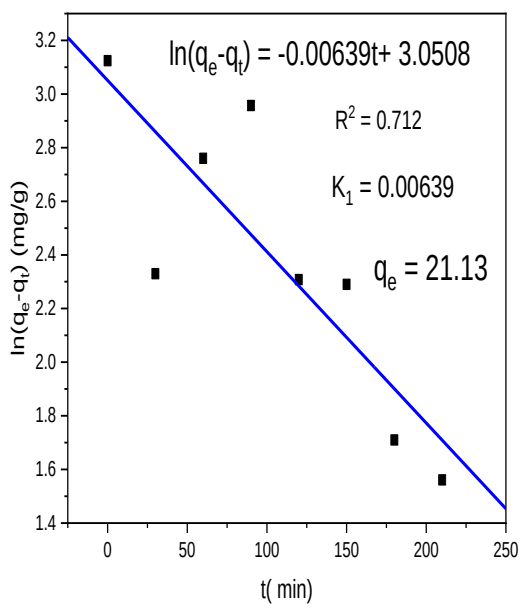

a)pseudo-first-order model

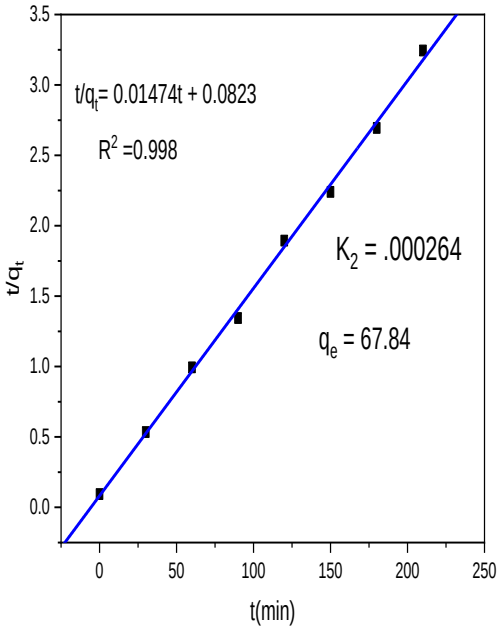

b) pseudo-second-order models

Figure 4. 13: Linear fitting model of a) pseudo first and b) pseudo second order

The pseudo-first-order and pseudo-second-order models in Figure 4.13 a show, a good fitting to the experimental data with R^2=0.712 and 0.998 for Fe(II) ions, respectively. Moreover, the theoretically calculated adsorption capacities from pseudo-first-order and pseudo-second-order models were found to be 21.13 and 67.84 mg/g, respectively, and the adsorption capacity obtained from the pseudo-second-order model is close to the experimental value. Hence, the pseudo-second-order model can be applied to predict the adsorption kinetics, and so that, the rate-controlling step was chemisorption (Q. Zhou et al., 2018).

4.9. Reusability study

To assess the durability of this adsorbent, reusability studies were carried out. The reusing efficiency of KOH-AC-WHL for four consecutive cycles is shown in Figure 4.14. To study reusability study 1g of adsorbent dose, 6 of pH of the solution, 50 mg/L of initial iron concentration at 90 min. contact time with removal efficiency of 99.3% contacted to regenerate adsorbent. As shown in bar graph figure 4.14, the removal efficiency of the first cycle was 91.5% while the second cycle resulted 75% and third cycle the removal efficiency of iron ion was 68 %

due to biochar become saturated with adsorbed substance, This value ensures that the prepared adsorbent could be reused different times without any loss of adsorption ability. Therefore, KOH-WHBC is a promising adsorbent for removal of iron ion from contaminant water. The reusability of the adsorbents is important for the economic feasibility and practical implications. As supported by literature(W. Ahmed et al., 2021), it can be generalized that if we use for 2 times KOH-AC-WHL is suitable for the re-adsorption iron from wastewater.

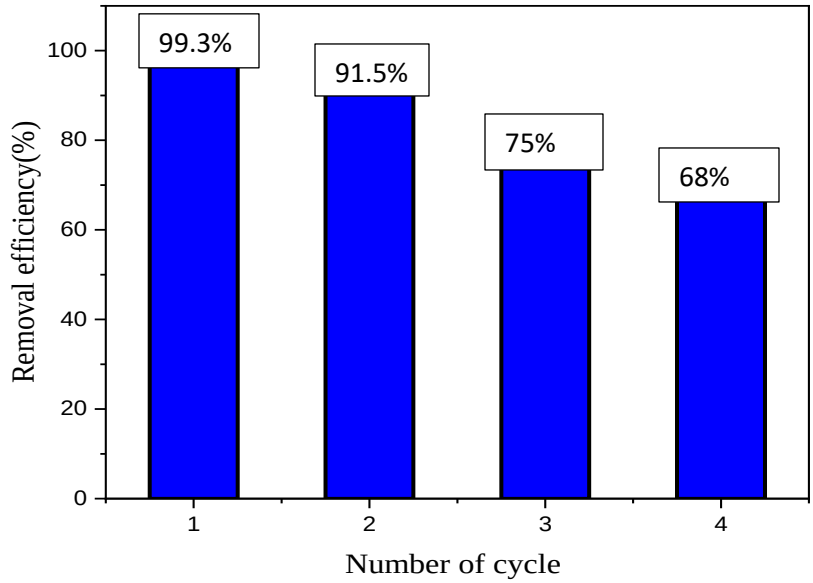

Figure 4. 14: KOH-AC-WHL recycling study

4.10. Removal of iron from Real water

The removal efficiency of the adsorbent drops to 70%, the result shows a significant decrement in the removal efficiency of the adsorbent due to the presence of a large amount of other heavy metals. Real water has complex and diverse compositions, including high concentrations of interfering substances, complex organic compounds, or heavy metals. These substances can compete with iron ions for adsorption sites on the adsorbent or form complexes that reduce the availability of active sites. This competition and interference can lead to a decrease in the removal efficiency. Moreover, real waste water contains suspended solids, colloidal matter, or organic compounds that can adhere to the surface of the adsorbent and form a fouling layer. This fouling layer can block or reduce the accessibility of the active sites, inhibiting effective iron removal.

4.11. Comparison of investigated adsorbents with other adsorbents

In this study, the adsorption capacities (calculated from Langmuir isotherm) of various adsorbents for Fe(II) were compared in Table 4.3 It could be concluded that activated carbon and modified activated carbon prepared from water hyacinth have higher adsorption capacities than the other types of adsorbents. In addition, the adsorption of Fe(II) by activated carbons is very fast. Thus, the modified activated carbons by KOH are promising adsorbents for iron removal from an aqueous solution.

Table 4. 3: Comparison of adsorption capacities of iron on different adsorbents

	Conditions					
Adsorbent	Fe	C_0(mg/L)	Dose	pH	Q_m(mg/g)	Reference
Corn cobs AC	III	5-40	0.1	8	500	(El-bendary et al., 2021)
Modified corn cobs AC	III	5-40	0.1	8	250	(El-bendary et al., 2021)
Olive stone waste AC	II	20	3	5	57.47	(Alslaibi et al., 2014)
Cross-linked chitosan beads	III	6	0.1	5	99.09	(Ngah et al., 2005)
Cross- linked chitosan beads	II	6	0.1	5	64.1	(Ngah et al., 2005)
Coir fibers	II	74	20	6.6	2.84	(Shukla et al., 2006)
Oxidized coir fibers	II	74	20	6	7.49	(Shukla et al., 2006)
Calabrian pine bark waste	II	55-111	10	4	2.03	(Acemioğlu, 2004)
Agrobacterium tumefacients	III	5-100	37.5	2.9	2.12	(Baytak & Türker, 2005)
Pretreated orange peel	III	30	1	3	18.2	(Lugo-Lugo et al., 2012)
Crude olive stone	III	5-100	37.5	2.9	1.2	(Nieto et al., 2010)
E.coli biofilm on kaolin	III	10-100	6.6	2.7-3.5	16.5	(Quintelas et al., 2009)
Streptomyces rimosus biomass	III	100	3	10	125	(Selatnia et al., 2004)
Pecan nutshell	III	200	4	4	76.6	(Vaghetti et al., 2009)
Egg shells	III	1-10	2.5	7	8.7	(Yeddou & Bensmaili, 2007)
lignite	II	130	6	3.5	34.22	(Mohan & Chander, 2006)
lignite	III	130	6	3.5	11.9	(Mohan & Chander, 2006)
KOH-AC-WHL	II	50-100	1	6	312.5	Present study

Chapter Five

5. Conclusions and Recommendations

5.1. Conclusion

The present investigation focused on the synthesis and characterization of KOH-AC-WHBC adsorbent from water hyacinth to remove iron from synthetic, and real wastewater effluent. KOH-AC-WHL is an effective adsorbent for the removal of Fe(II) ions from an aqueous solution. The removal of Fe(II) ions using KOH-AC-WHL was pH dependent and better adsorption capacity was obtained at pH 6.0, a contact time of 90 min, at an optimum adsorbent dose of 1 g/L, and calcination temperature of 500 ^{0}C suggesting that this is a reasonable and cost-effective adsorption technique. The XRD, FTIR, and SEM result analysis confirmed that iron was successfully adsorbed by KOH-AC-WHBC.

The experimental adsorption data were fitted to Langmuir and Freundlich isotherm models. Experimental results are in good agreement with the Langmuir adsorption isotherm model, with a maximum monolayer adsorption capacity of 312.5mg/g. The cost of Fe(II) ions removal using KOH-AC-WHL is quite low as the raw materials for the synthesized adsorbent are easily available in large amounts from highly invasive weeds. Moreover, this is a simple technique to control the spread of unwanted water hyacinth weed by utilization.

5.2. Recommendation

For future work, the following recommendations are suggested based on the results obtained from this study.

-It is recommended that to conduct response surface method in order to know the interaction effect of the parameter within each and as well as adsorption thermodynamics of the system.

-In this study batch adsorption experiment, equilibrium isotherm, and kinetics were conducted. However, further column adsorption study is recommended for a continuous flow system to optimize process design variables and scale up for practical applications.

-Further studies on the effectiveness of other regenerating solutions such as H_2SO_4, HCl, NaOH, and solvent methods will be recommended.

Reference

Abdullah, N., Yusof, N., Lau, W. J., Jaafar, J., & Ismail, A. F. (2019). Recent trends of heavy metal removal from water/wastewater by membrane technologies. *Journal of Industrial and Engineering Chemistry*, *76*, 17–38. https://doi.org/10.1016/j.jiec.2019.03.029

Acemioğlu, B. (2004). Removal of Fe(II) ions from aqueous solution by Calabrian pine bark wastes. *Bioresource Technology*, *93*(1), 99–102. https://doi.org/10.1016/j.biortech.2003.10.010

Ahmadi, M., Rahmani, H., Ramavandi, B., & Kakavandi, B. (2017). Removal of nitrate from aqueous solution using activated carbon modified with Fenton reagents. *Desalination and Water Treatment*, *76*, 265–275. https://doi.org/10.5004/dwt.2017.20705

Ahmed, N., Rahman, M., Won, S., & Shim, S. (2017). Biochar properties and eco-friendly applications for climate change mitigation , waste management , and wastewater treatment : A review. *Renewable and Sustainable Energy Reviews*, *79*(May), 255–273. https://doi.org/10.1016/j.rser.2017.05.057

Ahmed, W., Mehmood, S., Núñez-Delgado, A., Ali, S., Qaswar, M., Shakoor, A., Mahmood, M., & Chen, D. Y. (2021). Enhanced adsorption of aqueous Pb(II) by modified biochar produced through pyrolysis of watermelon seeds. *Science of the Total Environment*, *784*, 147136. https://doi.org/10.1016/j.scitotenv.2021.147136

Akendo, I. C. O., Gumbe, L. O., & Gitau, A. N. (2008). Dewatering and Drying Characteristics of Water Hyacinth (Eichhornia crassipes) Petiole. Part I. Dewatering Characteristics. *Agricultural Engineering International: CIGR Ejournal*, *X*, 1–11.

Alimohammadi, V., Sedighi, M., & Jabbari, E. (2017). Experimental study on efficient removal of total iron from wastewater using magnetic-modified multi-walled carbon nanotubes. *Ecological Engineering*, *102*, 90–97. https://doi.org/10.1016/j.ecoleng.2017.01.044

Allam, F., Elnouby, M., El-Khatib, K. M., El-Badan, D. E., & Sabry, S. A. (2020). Water hyacinth (Eichhornia crassipes) biochar as an alternative cathode electrocatalyst in an air-cathode single chamber microbial fuel cell. *International Journal of Hydrogen Energy*, *45*(10), 5911–5927. https://doi.org/10.1016/j.ijhydene.2019.09.164

Alslaibi, T. M., Abustan, I., Ahmad, M. A., & Foul, A. A. (2014). Kinetics and equilibrium adsorption of iron (II), lead (II), and copper (II) onto activated carbon prepared from olive stone waste. *Desalination and Water Treatment*, *52*(40–42), 7887–7897. https://doi.org/10.1080/19443994.2013.833875

Andersen, W. C., & Bruno, T. J. (2003). Application of a gas-liquid entraining rotor to supercritical fluid extraction: Removal of iron(III) from water. *Analytica Chimica Acta*, *485*(1), 1–8. https://doi.org/10.1016/S0003-2670(03)00400-8

Arora, R. (2019). ScienceDirect Adsorption of Heavy Metals – A Review. *Materials Today: Proceedings*, *18*, 4745–4750. https://doi.org/10.1016/j.matpr.2019.07.462

Aysu, T., & Küçük, M. M. (2014). Biomass pyrolysis in a fixed-bed reactor: Effects of pyrolysis parameters on product yields and characterization of products. *Energy*, *64*, 1002–1025. https://doi.org/10.1016/j.energy.2013.11.053

Barakat, M. A. (2011). New trends in removing heavy metals from industrial wastewater. *Arabian Journal of Chemistry*, *4*(4), 361–377. https://doi.org/10.1016/j.arabjc.2010.07.019

Baytak, S., & Türker, A. R. (2005). The use of Agrobacterium tumefacients immobilized on Amberlite XAD-4 as a new biosorbent for the column preconcentration of iron(III), cobalt(II), manganese(II) and chromium(III). *Talanta*, *65*(4), 938–945. https://doi.org/10.1016/j.talanta.2004.08.021

Belete, K., Getu, E., & Mekonnen, A. (2022). Investigation on Suitability and Safeness of Water hyacinth for Animal Feed, from Lake Ziway. *SINET: Ethiopian Journal of Science*, *45*(3), 283–295. https://doi.org/10.4314/sinet.v45i3.4

Ben, I., Antonopoulou, G., Ntaikou, I., Alexandropoulou, M., Nasri, M., Mechichi, T., & Lyberatos, G. (2019). Bioresource Technology On the evaluation of di ff erent sacchari fi cation schemes for enhanced bioethanol production from potato peels waste via a newly isolated yeast strain of Wickerhamomyces anomalus. *Bioresource Technology*, *289*(April), 121614. https://doi.org/10.1016/j.biortech.2019.121614

Beni, A. A., & Esmaeili, A. (2020). Biosorption, an efficient method for removing heavy metals from industrial effluents: A Review. In *Environmental Technology and Innovation* (Vol. 17). Elsevier B.V. https://doi.org/10.1016/j.eti.2019.100503

Bhatia, S. K., Jagtap, S. S., Bedekar, A. A., Bhatia, R. K., Patel, A. K., Pant, D., Rajesh Banu, J., Rao, C. V., Kim, Y. G., & Yang, Y. H. (2020). Recent developments in pretreatment technologies on lignocellulosic biomass: Effect of key parameters, technological improvements, and challenges. *Bioresource Technology*, *300*, 122724. https://doi.org/10.1016/j.biortech.2019.122724

Boyle, E. A., Edmond, J. M., & Sholkovitz, E. R. (1977). The mechanism of iron removal in estuaries. *Geochimica et Cosmochimica Acta*, *41*(9), 1313–1324. https://doi.org/10.1016/0016-7037(77)90075-8

Bulai, P., & Cioanca, E. (2005). Iron Removal From Wastewater Using Chelating Resin Purolite S930. *Tehnomus*, 1–6.

Burakov, A. E., Galunin, E. V., Burakova, I. V., Kucherova, A. E., Agarwal, S., Tkachev, A. G., & Gupta, V. K. (2018). Adsorption of heavy metals on conventional and nanostructured materials for wastewater treatment purposes: A review. *Ecotoxicology and Environmental Safety*, *148*(November 2017), 702–712. https://doi.org/10.1016/j.ecoenv.2017.11.034

Cai, C., Zhao, M., Yu, Z., Rong, H., & Zhang, C. (2019). Utilization of nanomaterials for in-situ remediation of heavy metal(loid) contaminated sediments: A review. *Science of the Total Environment*, *662*, 205–217. https://doi.org/10.1016/j.scitotenv.2019.01.180

Carreño-Sayago, U. F. (2021). Development of microspheres using water hyacinth (Eichhornia crassipes) for treatment of contaminated water with Cr(VI). *Environment, Development and Sustainability*, *23*(3), 4735–4746. https://doi.org/10.1007/s10668-020-00776-0

Chaturvedi, S., & Dave, P. N. (2012). Removal of iron for safe drinking water. *Desalination*, *303*, 1–11. https://doi.org/10.1016/j.desal.2012.07.003

Chau, M. Q., Truong, T. T., Hoang, A. T., & Le, T. H. (2021). Oil spill cleanup by raw cellulose-

based absorbents: a green and sustainable approach. *Energy Sources, Part A: Recovery, Utilization and Environmental Effects*, *00*(00), 1–14. https://doi.org/10.1080/15567036.2021.1928798

Chen, Q. (2010). Study on the adsorption of lanthanum(III) from aqueous solution by bamboo charcoal. *Journal of Rare Earths*, *28*(SUPPL. 1), 125–131. https://doi.org/10.1016/S1002-0721(10)60272-4

Chen, W., Wei, R., Ni, J., Yang, L., Qian, W., & Yang, Y. (2018). Sorption of chlorinated hydrocarbons to biochars in aqueous environment: Effects of the amorphous carbon structure of biochars and the molecular properties of adsorbates. *Chemosphere*, *210*, 753–761. https://doi.org/10.1016/j.chemosphere.2018.07.071

Chen, Z., Rao, Y., Usman, M., Chen, H., Białowiec, A., Zhang, S., & Luo, G. (2021). Anaerobic fermentation of hydrothermal liquefaction wastewater of dewatered sewage sludge for volatile fatty acids production with focuses on the degradation of organic components and microbial community compositions. *Science of the Total Environment*, *777*. https://doi.org/10.1016/j.scitotenv.2021.146077

Choo, K. H., Lee, H., & Choi, S. J. (2005). Iron and manganese removal and membrane fouling during UF in conjunction with prechlorination for drinking water treatment. *Journal of Membrane Science*, *267*(1–2), 18–26. https://doi.org/10.1016/j.memsci.2005.05.021

Chua, Y. W., Wu, H., & Yu, Y. (2019). Interactions between Low- and High-Molecular-Weight Portions of Lignin during Fast Pyrolysis at Low Temperatures [Research-article]. *Energy & Fuels*, *33*, 11173–11180. https://doi.org/10.1021/acs.energyfuels.9b02813

Da Silva Correia, I. K., Santos, P. F., Santana, C. S., Neris, J. B., Luzardo, F. H. M., & Velasco, F. G. (2018). Application of coconut shell, banana peel, spent coffee grounds, eucalyptus bark, piassava (Attalea funifera) and water hyacinth (Eichornia crassipes) in the adsorption of Pb2+ and Ni2+ ions in water. *Journal of Environmental Chemical Engineering*, *6*(2), 2319–2334. https://doi.org/10.1016/j.jece.2018.03.033

Dąbrowski, A., Hubicki, Z., Podkościelny, P., & Robens, E. (2004). Selective removal of the heavy metal ions from waters and industrial wastewaters by ion-exchange method. *Chemosphere*, *56*(2), 91–106. https://doi.org/10.1016/j.chemosphere.2004.03.006

Ding, Y., Zhang, J., He, Q., Huang, B., & Mao, S. (2019). The application and validity of various reaction kinetic models on woody biomass pyrolysis. *Energy*, *179*, 784–791. https://doi.org/10.1016/j.energy.2019.05.021

Dong, X., Ma, L. Q., & Li, Y. (2011). Characteristics and mechanisms of hexavalent chromium removal by biochar from sugar beet tailing. *Journal of Hazardous Materials*, *190*(1–3), 909–915. https://doi.org/10.1016/j.jhazmat.2011.04.008

Du, Y., Wu, Q., Kong, D., Shi, Y., Huang, X., Luo, D., Chen, Z., Xiao, T., & Leung, J. Y. S. (2020). Accumulation and translocation of heavy metals in water hyacinth: Maximising the use of green resources to remediate sites impacted by e-waste recycling activities. *Ecological Indicators*, *115*(April), 106384. https://doi.org/10.1016/j.ecolind.2020.106384

El-bendary, N., El-etriby, H. K., & Mahanna, H. (2021). *High-performance removal of iron from*

aqueous solution using modified activated carbon prepared from corn cobs and luffa sponge. *213*, 348–357. https://doi.org/10.5004/dwt.2021.26721

El-Naggar, H. M. (2010). Development of low-cost technology for the removal of iron and manganese from ground water in siwa oasis. *The Journal of the Egyptian Public Health Association*, *85*(3–4), 169–188. http://www.ncbi.nlm.nih.gov/pubmed/21244816

Engineering, P., Island, W., & State, B. (2019). *Characterization Of Water Hyacinth (Eichhornia Crassipes) For The Production Of Thermochemical Fuels*. *5*(7), 2661–2665.

Fallavena, V. L. V., De Abreu, C. S., Inácio, T. D., Azevedo, C. M. N., Pires, M., Ferret, L. S., Fernandes, I. D., & Tarazona, R. M. (2014). Determination of mineral matter in Brazilian coals by thermal treatments. *Fuel Processing Technology*, *125*, 41–50. https://doi.org/10.1016/j.fuproc.2014.03.018

Febrianto, J., Kosasih, A. N., Sunarso, J., Ju, Y. H., Indraswati, N., & Ismadji, S. (2009). Equilibrium and kinetic studies in adsorption of heavy metals using biosorbent: A summary of recent studies. *Journal of Hazardous Materials*, *162*(2–3), 616–645. https://doi.org/10.1016/j.jhazmat.2008.06.042

Feng, Z., & Zhu, L. (2018). Sorption of phenanthrene to biochar modified by base. *Frontiers of Environmental Science and Engineering*, *12*(2), 1–11. https://doi.org/10.1007/s11783-017-0978-7

Gan, M., Zheng, Z., Sun, S., Zhu, J., & Liu, X. (2015). The influence of aluminum chloride on biosynthetic schwertmannite and Cu(ii)/Cr(vi) adsorption. *RSC Advances*, *5*(114), 94500–94512. https://doi.org/10.1039/c5ra17316g

Gaurav, G. K., Mehmood, T., Cheng, L., Klemeš, J. J., & Shrivastava, D. K. (2020). Water hyacinth as a biomass: A review. *Journal of Cleaner Production*, *277*, 122214. https://doi.org/10.1016/j.jclepro.2020.122214

Ghosh, D., Solanki, H., & Purkait, M. K. (2008). Removal of Fe(II) from tap water by electrocoagulation technique. *Journal of Hazardous Materials*, *155*(1–2), 135–143. https://doi.org/10.1016/j.jhazmat.2007.11.042

Gong, H., Tan, Z., Huang, K., Zhou, Y., Yu, J., & Huang, Q. (2021). Mechanism of cadmium removal from soil by silicate composite biochar and its recycling. *Journal of Hazardous Materials*, *409*(June 2020), 125022. https://doi.org/10.1016/j.jhazmat.2020.125022

Group, S. P. (2016). *Heavy Metals Contamination in Agricultural Soil and Rice in Tanzania : A Review Tanzania : A Review*. https://doi.org/10.11648/j.ijepp.20160401.13

Gupta, S., Sireesha, S., Sreedhar, I., Patel, C. M., & Anitha, K. L. (2020). Latest trends in heavy metal removal from wastewater by biochar based sorbents. *Journal of Water Process Engineering*, *38*(October), 101561. https://doi.org/10.1016/j.jwpe.2020.101561

He, R., Peng, Z., Lyu, H., Huang, H., Nan, Q., & Tang, J. (2018). Synthesis and characterization of an iron-impregnated biochar for aqueous arsenic removal. *Science of the Total Environment*, *612*, 1177–1186. https://doi.org/10.1016/j.scitotenv.2017.09.016

Hemalatha, D., Narayanan, R. M., & Sanchitha, S. (2020). Removal of Zinc and Chromium from

industrial wastewater using water hyacinth (E. crassipes) petiole, leaves and root powder: Equilibrium study. *Materials Today: Proceedings*, *43*(December), 1834–1838. https://doi.org/10.1016/j.matpr.2020.10.725

Ho, K., Kim, J., Cho, T., & Weon, J. (2012). Bioresource Technology Influence of pyrolysis temperature on physicochemical properties of biochar obtained from the fast pyrolysis of pitch pine (Pinus rigida). *BIORESOURCE TECHNOLOGY*, *118*, 158–162. https://doi.org/10.1016/j.biortech.2012.04.094

Hoang, A. T., Nižetić, S., Cheng, C. K., Luque, R., Thomas, S., Banh, T. L., Pham, V. V., & Nguyen, X. P. (2022). Heavy metal removal by biomass-derived carbon nanotubes as a greener environmental remediation: A comprehensive review. In *Chemosphere* (Vol. 287, Issue August 2021). https://doi.org/10.1016/j.chemosphere.2021.131959

Hoang, A. T., Nižetić, S., Duong, X. Q., Rowinski, L., & Nguyen, X. P. (2021). Advanced super-hydrophobic polymer-based porous absorbents for the treatment of oil-polluted water. *Chemosphere*, *277*. https://doi.org/10.1016/j.chemosphere.2021.130274

Hoang, A. T., & Pham, X. D. (2021). An investigation of remediation and recovery of oil spill and toxic heavy metal from maritime pollution by a new absorbent material. *Journal of Marine Engineering and Technology*, *20*(3), 159–169. https://doi.org/10.1080/20464177.2018.1544401

Honlah, E., Segbefia, A. Y., Appiah, D. O., & Mensah, M. (2019). The Effects of Water Hyacinth Invasion on Smallholder Farming along River Tano and Tano Lagoon, Ghana. *Cogent Food and Agriculture*, *5*(1). https://doi.org/10.1080/23311932.2019.1567042

Hu, K., Xu, D., & Chen, Y. (2020). An assessment of sulfate reducing bacteria on treating sulfate-rich metal-laden wastewater from electroplating plant. *Journal of Hazardous Materials*, *393*(February), 122376. https://doi.org/10.1016/j.jhazmat.2020.122376

Huang, F., Gao, L. Y., Deng, J. H., Chen, S. H., & Cai, K. Z. (2018). Quantitative contribution of Cd2+ adsorption mechanisms by chicken-manure-derived biochars. *Environmental Science and Pollution Research*, *25*(28), 28322–28334. https://doi.org/10.1007/s11356-018-2889-y

Huang, Y., Li, S., Chen, J., Zhang, X., & Chen, Y. (2014). Adsorption of Pb(II) on mesoporous activated carbons fabricated from water hyacinth using H 3 PO 4 activation: Adsorption capacity, kinetic and isotherm studies. *Applied Surface Science*, *293*, 160–168. https://doi.org/10.1016/j.apsusc.2013.12.123

Itoh, Y., Bröcker, M. J., Sekine, S. I., Söll, D., & Yokoyama, S. (2014). Dimer-dimer interaction of the bacterial selenocysteine synthase sela promotes functional active-site formation and catalytic specificity. *Journal of Molecular Biology*, *426*(8), 1723–1735. https://doi.org/10.1016/j.jmb.2014.01.003

Johnson, K. L., & Younger, P. L. (2006). The co-treatment of sewage and mine waters in aerobic wetlands. *Engineering Geology*, *85*(1–2), 53–61. https://doi.org/10.1016/j.enggeo.2005.09.026

Kibret, e. A., & science, a. (2023). *An investigation on the removal of iron and chromium from steel industry effluent by an investigation on the removal of iron and chromium from steel*

industry effluent by adsorption process.

Kołtowski, M., Hilber, I., Bucheli, T. D., Charmas, B., Skubiszewska-Zięba, J., & Oleszczuk, P. (2017). Activated biochars reduce the exposure of polycyclic aromatic hydrocarbons in industrially contaminated soils. *Chemical Engineering Journal*, *310*, 33–40. https://doi.org/10.1016/j.cej.2016.10.065

Kong, Q., He, X., Shu, L., & Miao, M. sheng. (2017). Ofloxacin adsorption by activated carbon derived from luffa sponge: Kinetic, isotherm, and thermodynamic analyses. *Process Safety and Environmental Protection*, *112*, 254–264. https://doi.org/10.1016/j.psep.2017.05.011

Kumar, A., Joseph, S., Tsechansky, L., Privat, K., Schreiter, I. J., Schüth, C., & Graber, E. R. (2018). Biochar aging in contaminated soil promotes Zn immobilization due to changes in biochar surface structural and chemical properties. *Science of the Total Environment*, *626*, 953–961. https://doi.org/10.1016/j.scitotenv.2018.01.157

Kumar, M., Nandi, M., & Pakshirajan, K. (2021). Recent advances in heavy metal recovery from wastewater by biogenic sulfide precipitation. *Journal of Environmental Management*, *278*(P2), 111555. https://doi.org/10.1016/j.jenvman.2020.111555

Kumar, V., & Dwivedi, S. K. (2021). A review on accessible techniques for removal of hexavalent Chromium and divalent Nickel from industrial wastewater : Recent research and future outlook. *Journal of Cleaner Production*, *295*, 126229. https://doi.org/10.1016/j.jclepro.2021.126229

Lakherwal, D. (2014). *Adsorption of Heavy Metals : A Review*. *4*(1), 41–48.

Lei, T., Li, S. J., Jiang, F., Ren, Z. X., Wang, L. L., Yang, X. J., Tang, L. H., & Wang, S. X. (2019). Adsorption of Cadmium Ions from an Aqueous Solution on a Highly Stable Dopamine-Modified Magnetic Nano-Adsorbent. *Nanoscale Research Letters*, *14*(1). https://doi.org/10.1186/s11671-019-3154-0

Leng, L., Huang, H., Li, H., Li, J., & Zhou, W. (2019). Biochar stability assessment methods: A review. *Science of the Total Environment*, *647*, 210–222. https://doi.org/10.1016/j.scitotenv.2018.07.402

Ley 25.632. (2002). *済無No Title No Title No Title*. *36*(4), 935–948.

Li, H., Xiong, J., Zhang, G., Liang, A., Long, J., & Xiao, T. (2020). Science of the Total Environment Enhanced thallium (I) removal from wastewater using hypochlorite oxidation coupled with magnetite-based biochar adsorption. *Science of the Total Environment*, *698*, 134166. https://doi.org/10.1016/j.scitotenv.2019.134166

Li, M., Liu, H., Chen, T., Dong, C., & Sun, Y. (2019). Synthesis of magnetic biochar composites for enhanced uranium(VI) adsorption. *Science of the Total Environment*, *651*, 1020–1028. https://doi.org/10.1016/j.scitotenv.2018.09.259

Li, Y., Du, Q., Wang, X., Zhang, P., Wang, D., Wang, Z., & Xia, Y. (2010). Removal of lead from aqueous solution by activated carbon prepared from Enteromorpha prolifera by zinc chloride activation. *Journal of Hazardous Materials*, *183*(1–3), 583–589. https://doi.org/10.1016/j.jhazmat.2010.07.063

Li, Z., Xing, B., Ding, Y., Li, Y., & Wang, S. (2020). A high-performance biochar produced from bamboo pyrolysis with in-situ nitrogen doping and activation for adsorption of phenol and methylene blue. *Chinese Journal of Chemical Engineering*, *28*(11), 2872–2880. https://doi.org/10.1016/j.cjche.2020.03.031

Lian, G., Wang, B., Lee, X., Li, L., Liu, T., & Lyu, W. (2019). Enhanced removal of hexavalent chromium by engineered biochar composite fabricated from phosphogypsum and distillers grains. *Science of the Total Environment*, *697*, 134119. https://doi.org/10.1016/j.scitotenv.2019.134119

Lin, L., Yan, R., Liu, Y., & Jiang, W. (2010). In-depth investigation of enzymatic hydrolysis of biomass wastes based on three major components: Cellulose, hemicellulose and lignin. *Bioresource Technology*, *101*(21), 8217–8223. https://doi.org/10.1016/j.biortech.2010.05.084

Liu, C., Ye, J., Lin, Y., Wu, J., Price, G. W., Burton, D., & Wang, Y. (2020). Removal of Cadmium (II) using water hyacinth (Eichhornia crassipes) biochar alginate beads in aqueous solutions. *Environmental Pollution*, *264*, 114785. https://doi.org/10.1016/j.envpol.2020.114785

Liu, L., Pang, Y., Lv, D., Wang, K., & Wang, Y. (2021). Thermal and kinetic analyzing of pyrolysis and combustion of self-heating biomass particles. *Process Safety and Environmental Protection*, *151*, 39–50. https://doi.org/10.1016/j.psep.2021.05.011

Liu, Z., Fu, X., Li, M., Wang, F., Wang, Q., Kang, G., & Peng, F. (2015). Novel silicon-doped, silicon and nitrogen-codoped carbon nanomaterials with high activity for the oxygen reduction reaction in alkaline medium. *Journal of Materials Chemistry A*, *3*(7), 3289–3293. https://doi.org/10.1039/c4ta05937a

Lu, X., Kruatrachue, M., Pokethitiyook, P., & Homyok, K. (2004). *V30_093_103*. *30*, 93–103.

Lugo-Lugo, V., Barrera-Díaz, C., Ureña-Núñez, F., Bilyeu, B., & Linares-Hernández, I. (2012). Biosorption of Cr(III) and Fe(III) in single and binary systems onto pretreated orange peel. *Journal of Environmental Management*, *112*, 120–127. https://doi.org/10.1016/j.jenvman.2012.07.009

Maniscalco, M. P., Volpe, M., & Messineo, A. (2020). *Hydrothermal Carbonization as a Valuable Tool for Energy and Environmental Applications : A Review*.

Mao, Q., Zhou, Y., Yang, Y., Zhang, J., Liang, L., & Wang, H. (2019). Experimental and theoretical aspects of biochar-supported nanoscale zero- valent iron activating H 2 O 2 for cipro fl oxacin removal from aqueous solution. *Journal of Hazardous Materials*, *380*(July), 120848. https://doi.org/10.1016/j.jhazmat.2019.120848

Márquez-Montesino, F., Correa-Méndez, F., Glauco-Sánchez, C., Zanzi-Vigouroux, R., Rutiaga-Quiñones, J. G., & Aguiar-Trujillo, L. (2015). Pyrolytic degradation studies of acacia mangium wood. *BioResources*, *10*(1), 1825–1844. https://doi.org/10.15376/biores.10.1.1825-1844

Martínez-Huitle, C. A., & Panizza, M. (2018). Electrochemical oxidation of organic pollutants for wastewater treatment. *Current Opinion in Electrochemistry*, *11*, 62–71.

https://doi.org/10.1016/j.coelec.2018.07.010

Martins, D., Rocha, C., Dourado, F., & Gama, M. (2021). Bacterial Cellulose-Carboxymethyl Cellulose (BC:CMC) dry formulation as stabilizer and texturizing agent for surfactant-free cosmetic formulations. *Colloids and Surfaces A: Physicochemical and Engineering Aspects*, *617*(September 2020), 126380. https://doi.org/10.1016/j.colsurfa.2021.126380

Masto, R. E., Kumar, S., Rout, T. K., Sarkar, P., George, J., & Ram, L. C. (2013). Biochar from water hyacinth (Eichornia crassipes) and its impact on soil biological activity. *Catena*, *111*, 64–71. https://doi.org/10.1016/j.catena.2013.06.025

Mohan, D., & Chander, S. (2006). Single, binary, and multicomponent sorption of iron and manganese on lignite. *Journal of Colloid and Interface Science*, *299*(1), 76–87. https://doi.org/10.1016/j.jcis.2006.02.010

Mohan, D., & Pittman, C. U. (2007). Arsenic removal from water/wastewater using adsorbents-A critical review. *Journal of Hazardous Materials*, *142*(1–2), 1–53. https://doi.org/10.1016/j.jhazmat.2007.01.006

Mohan, D., Pittman, C. U., & Steele, P. H. (2006). *Pyrolysis of Wood / Biomass for Bio-oil : A Critical Review*. *4*, 848–889.

Mohanty, S. K., Valenca, R., Berger, A. W., Yu, I. K. M., Xiong, X., Saunders, T. M., & Tsang, D. C. W. (2018). Plenty of room for carbon on the ground: Potential applications of biochar for stormwater treatment. *Science of the Total Environment*, *625*, 1644–1658. https://doi.org/10.1016/j.scitotenv.2018.01.037

Moradi, O., & Zare, K. (2013). Adsorption of ammonium ion by multi-walled carbon nanotube: Kinetics and thermodynamic studies. *Fullerenes Nanotubes and Carbon Nanostructures*, *21*(6), 449–459. https://doi.org/10.1080/1536383X.2011.613538

Nallakukkala, S., Lal, B., & Shaik, F. (2021). Kinetic and isothermal investigations in elimination of iron metal from aqueous mixture by using natural adsorbent. *International Journal of Environmental Science and Technology*, *18*(7), 1761–1772. https://doi.org/10.1007/s13762-020-02919-2

Neris, J. B., Luzardo, F. H. M., Santos, P. F., De Almeida, O. N., & Velasco, F. G. (2019). Evaluation of single and tri-element adsorption of Pb 2+ , Ni 2+ and Zn 2+ ions in aqueous solution on modified water hyacinth (Eichhornia crassipes) fibers. *Journal of Environmental Chemical Engineering*, *7*(1), 102885. https://doi.org/10.1016/j.jece.2019.102885

Ngah, W. S. W., Ab Ghani, S., & Kamari, A. (2005). Adsorption behaviour of Fe(II) and Fe(III) ions in aqueous solution on chitosan and cross-linked chitosan beads. *Bioresource Technology*, *96*(4), 443–450. https://doi.org/10.1016/j.biortech.2004.05.022

Nieto, L. M., Alami, S. B. D., Hodaifa, G., Faur, C., Rodríguez, S., Giménez, J. A., & Ochando, J. (2010). Adsorption of iron on crude olive stones. *Industrial Crops and Products*, *32*(3), 467–471. https://doi.org/10.1016/j.indcrop.2010.06.017

Nyamunda, B. C., Chivhanga, T., Guyo, U., & Chigondo, F. (2019). Removal of Zn (II) and Cu (II) Ions from Industrial Wastewaters Using Magnetic Biochar Derived from Water Hyacinth. *Journal of Engineering (United Kingdom)*, *2019*.

https://doi.org/10.1155/2019/5656983

Obernberger, I., Brunner, T., & Bärnthaler, G. (2006). Chemical properties of solid biofuels-significance and impact. *Biomass and Bioenergy*, *30*(11), 973–982. https://doi.org/10.1016/j.biombioe.2006.06.011

Olaolu, T. D., Akpor, O. B., & Akor, C. O. (2014). *Pollution indicators and pathogenic microorganisms in wastewater treatment : Implication on receiving water bodies*. *2*(6), 205–212. https://doi.org/10.11648/j.ijepp.20140206.12

Panwar, N. L., & Pawar, A. (2022). Influence of activation conditions on the physicochemical properties of activated biochar: a review. *Biomass Conversion and Biorefinery*, *12*(3), 925–947. https://doi.org/10.1007/s13399-020-00870-3

Papari, S., Hawboldt, K., & Helleur, R. (2015). Pyrolysis: A theoretical and experimental study on the conversion of softwood sawmill residues to biooil. *Industrial and Engineering Chemistry Research*, *54*(2), 605–611. https://doi.org/10.1021/ie5039456

Park, J. H., Ok, Y. S., Kim, S. H., Cho, J. S., Heo, J. S., Delaune, R. D., & Seo, D. C. (2016). Competitive adsorption of heavy metals onto sesame straw biochar in aqueous solutions. *Chemosphere*, *142*, 77–83. https://doi.org/10.1016/j.chemosphere.2015.05.093

Pashai Gatabi, M., Milani Moghaddam, H., & Ghorbani, M. (2016). Point of zero charge of maghemite decorated multiwalled carbon nanotubes fabricated by chemical precipitation method. *Journal of Molecular Liquids*, *216*, 117–125. https://doi.org/10.1016/j.molliq.2015.12.087

Patel, S. (2012). Threats, management and envisaged utilizations of aquatic weed Eichhornia crassipes: An overview. *Reviews in Environmental Science and Biotechnology*, *11*(3), 249–259. https://doi.org/10.1007/s11157-012-9289-4

Peng, W., Li, H., Liu, Y., & Song, S. (2017). A review on heavy metal ions adsorption from water by graphene oxide and its composites. *Journal of Molecular Liquids*, *230*, 496–504. https://doi.org/10.1016/j.molliq.2017.01.064

Prabakar, D., Manimudi, V. T., K, S. S., & Sampath, S. (2018). Advanced biohydrogen production using pretreated industrial waste : Outlook and prospects. *Renewable and Sustainable Energy Reviews*, *96*(August 2017), 306–324. https://doi.org/10.1016/j.rser.2018.08.006

Premarathna, K. S. D., Rajapaksha, A. U., Sarkar, B., Kwon, E. E., Bhatnagar, A., Ok, Y. S., & Vithanage, M. (2019). Biochar-based engineered composites for sorptive decontamination of water: A review. *Chemical Engineering Journal*, *372*(April), 536–550. https://doi.org/10.1016/j.cej.2019.04.097

Quintelas, C., Rocha, Z., Silva, B., Fonseca, B., Figueiredo, H., & Tavares, T. (2009). Removal of Cd(II), Cr(VI), Fe(III) and Ni(II) from aqueous solutions by an E. coli biofilm supported on kaolin. *Chemical Engineering Journal*, *149*(1–3), 319–324. https://doi.org/10.1016/j.cej.2008.11.025

Rajapaksha, A. U., Chen, S. S., Tsang, D. C. W., Zhang, M., Vithanage, M., Mandal, S., Gao, B., Bolan, N. S., & Ok, Y. S. (2016). Engineered/designer biochar for contaminant

removal/immobilization from soil and water: Potential and implication of biochar modification. *Chemosphere*, *148*, 276–291. https://doi.org/10.1016/j.chemosphere.2016.01.043

Rattanaphan, S., Rungrotmongkol, T., & Kongsune, P. (2020). Biogas improving by adsorption of CO2 on modified waste tea activated carbon. *Renewable Energy*, *145*, 622–631. https://doi.org/10.1016/j.renene.2019.05.104

Rezania, S., Oryani, B., Cho, J., Talaiekhozani, A., Sabbagh, F., Hashemi, B., Rupani, P. F., & Mohammadi, A. A. (2020). Different pretreatment technologies of lignocellulosic biomass for bioethanol production: An overview. *Energy*, *199*, 117457. https://doi.org/10.1016/j.energy.2020.117457

Rezania, S., Ponraj, M., Talaiekhozani, A., Mohamad, S. E., Md Din, M. F., Taib, S. M., Sabbagh, F., & Sairan, F. M. (2015). Perspectives of phytoremediation using water hyacinth for removal of heavy metals, organic and inorganic pollutants in wastewater. *Journal of Environmental Management*, *163*, 125–133. https://doi.org/10.1016/j.jenvman.2015.08.018

Rwiza, M. J., Oh, S., Kim, K., & Kim, S. D. (2018). AC SC. *ECSN*, *Ii*. https://doi.org/10.1016/j.chemosphere.2017.12.043

Sahoo, K., Kumar, A., & Chakraborty, J. P. (2021). A comparative study on valuable products: bio-oil, biochar, non-condensable gases from pyrolysis of agricultural residues. *Journal of Material Cycles and Waste Management*, *23*(1), 186–204. https://doi.org/10.1007/s10163-020-01114-2

Sanmuga Priya, E., & Senthamil Selvan, P. (2017). Water hyacinth (Eichhornia crassipes) – An efficient and economic adsorbent for textile effluent treatment – A review. *Arabian Journal of Chemistry*, *10*, S3548–S3558. https://doi.org/10.1016/j.arabjc.2014.03.002

Selatnia, A., Boukazoula, A., Kechid, N., Bakhti, M. Z., Chergui, A., & Kerchich, Y. (2004). Biosorption of lead (II) from aqueous solution by a bacterial dead Streptomyces rimosus biomass. *Biochemical Engineering Journal*, *19*(2), 127–135. https://doi.org/10.1016/j.bej.2003.12.007

Shaaban, A., Se, S. M., Mitan, N. M. M., & Dimin, M. F. (2013). Characterization of biochar derived from rubber wood sawdust through slow pyrolysis on surface porosities and functional groups. *Procedia Engineering*, *68*, 365–371. https://doi.org/10.1016/j.proeng.2013.12.193

Shah, K., Gupta, K., & Sengupta, B. (2017). Selective separation of copper and zinc from spent chloride brass pickle liquors using solvent extraction and metal recovery by precipitation-stripping. *Journal of Environmental Chemical Engineering*, *5*(5), 5260–5269. https://doi.org/10.1016/j.jece.2017.09.061

Sharma, H. K., Xu, C., & Qin, W. (2019). Biological Pretreatment of Lignocellulosic Biomass for Biofuels and Bioproducts: An Overview. *Waste and Biomass Valorization*, *10*(2), 235–251. https://doi.org/10.1007/s12649-017-0059-y

Shavandi, M. A., Haddadian, Z., Ismail, M. H. S., Abdullah, N., & Abidin, Z. Z. (2012). Removal of Fe(III), Mn(II) and Zn(II) from palm oil mill effluent (POME) by natural

zeolite. *Journal of the Taiwan Institute of Chemical Engineers*, *43*(5), 750–759. https://doi.org/10.1016/j.jtice.2012.02.014

Shen, Y., Zhu, W., Li, H., Ho, S. H., Chen, J., Xie, Y., & Shi, X. (2018). Enhancing cadmium bioremediation by a complex of water-hyacinth derived pellets immobilized with Chlorella sp. *Bioresource Technology*, *257*, 157–163. https://doi.org/10.1016/j.biortech.2018.02.060

Shukla, S. R., Pai, R. S., & Shendarkar, A. D. (2006). Adsorption of Ni(II), Zn(II) and Fe(II) on modified coir fibres. *Separation and Purification Technology*, *47*(3), 141–147. https://doi.org/10.1016/j.seppur.2005.06.014

Sizmur, T., Fresno, T., Akgül, G., Frost, H., & Moreno-Jiménez, E. (2017). Biochar modification to enhance sorption of inorganics from water. *Bioresource Technology*, *246*, 34–47. https://doi.org/10.1016/j.biortech.2017.07.082

Štembal, T., Markić, M., Ribičić, N., Briški, F., & Sipos, L. (2005). Removal of ammonia, iron and manganese from groundwaters of northern Croatia - Pilot plant studies. *Process Biochemistry*, *40*(1), 327–335. https://doi.org/10.1016/j.procbio.2004.01.006

Sukarni, Sudjito, Hamidi, N., Yanuhar, U., & Wardana, I. N. G. (2014). Potential and properties of marine microalgae Nannochloropsis oculata as biomass fuel feedstock. *International Journal of Energy and Environmental Engineering*, *5*(4), 279–290. https://doi.org/10.1007/s40095-014-0138-9

Tahir, S. S., & Rauf, N. (2004). Removal of Fe(II) from the wastewater of a galvanized pipe manufacturing industry by adsorption onto bentonite clay. *Journal of Environmental Management*, *73*(4), 285–292. https://doi.org/10.1016/j.jenvman.2004.06.009

Tan, X., Liu, Y., Zeng, G., Wang, X., Hu, X., & Gu, Y. (2015). Chemosphere Application of biochar for the removal of pollutants from aqueous solutions. *CHEMOSPHERE*. https://doi.org/10.1016/j.chemosphere.2014.12.058

Tchounwou, P. B., Yedjou, C. G., Patlolla, A. K., & Sutton, D. J. (n.d.). *Heavy Metal Toxicity and the Environment*. https://doi.org/10.1007/978-3-7643-8340-4

Téllez, T. R., López, E. M. de R., Granado, G. L., Pérez, E. A., López, R. M., & Guzmán, J. M. S. (2008). The water hyacinth, Eichhornia crassipes: An invasive plant in the Guadiana River Basin (Spain). *Aquatic Invasions*, *3*(1), 42–53. https://doi.org/10.3391/ai.2008.3.1.8

Uchimiya, M., Bannon, D. I., Wartelle, L. H., Lima, I. M., & Klasson, K. T. (2012). Lead retention by broiler litter biochars in small arms range soil: Impact of pyrolysis temperature. *Journal of Agricultural and Food Chemistry*, *60*(20), 5035–5044. https://doi.org/10.1021/jf300825n

Usman, M., Chen, H., Chen, K., Ren, S., Clark, J. H., Fan, J., Luo, G., & Zhang, S. (2019). Characterization and utilization of aqueous products from hydrothermal conversion of biomass for bio-oil and hydro-char production: A review. *Green Chemistry*, *21*(7), 1553–1572. https://doi.org/10.1039/c8gc03957g

Vaghetti, J. C. P., Lima, E. C., Royer, B., Cardoso, N. F., Martins, B., & Calvete, T. (2009). Pecan nutshell as biosorbent to remove toxic metals from aqueous solution. *Separation Science and Technology*, *44*(3), 615–644. https://doi.org/10.1080/01496390802634331

Vardhan, K. H., Kumar, P. S., & Panda, R. C. (2019). A review on heavy metal pollution, toxicity and remedial measures: Current trends and future perspectives. *Journal of Molecular Liquids*, *290*, 111197. https://doi.org/10.1016/j.molliq.2019.111197

Volpe, D., Tobiason, J., & Kaminski, G. (2012). Assessment of iron and manganese sequestration. *American Water Works Association Annual Conference and Exposition 2012, ACE 2012*, 4319–4333.

Wan, J., Liu, L., Ayub, K. S., Zhang, W., Shen, G., Hu, S., & Qian, X. (2020). Characterization and adsorption performance of biochars derived from three key biomass constituents. *Fuel*, *269*(October 2019), 117142. https://doi.org/10.1016/j.fuel.2020.117142

Wang, H., Feng, M., Zhou, F., Huang, X., Tsang, D. C. W., & Zhang, W. (2017). Effects of atmospheric ageing under different temperatures on surface properties of sludge-derived biochar and metal/metalloid stabilization. *Chemosphere*, *184*, 176–184. https://doi.org/10.1016/j.chemosphere.2017.05.175

Wang, J., Shi, L., Zhai, L., Zhang, H., Wang, S., Zou, J., Shen, Z., Lian, C., & Chen, Y. (2021). Analysis of the long-term effectiveness of biochar immobilization remediation on heavy metal contaminated soil and the potential environmental factors weakening the remediation effect: A review. *Ecotoxicology and Environmental Safety*, *207*(August 2020), 111261. https://doi.org/10.1016/j.ecoenv.2020.111261

Wang, Y. N., Liu, Q., Shu, L., Miao, M. S., Liu, Y. Z., & Kong, Q. (2016). Removal of Cr(VI) from aqueous solution using Fe-modified activated carbon prepared from luffa sponge: kinetic, thermodynamic, and isotherm studies. *Desalination and Water Treatment*, *57*(60), 29467–29478. https://doi.org/10.1080/19443994.2016.1185745

Waqas, M., Aburiazaiza, A. S., Minadad, R., Rehan, M., Barakat, M. A., & Nizami, A. S. (2018). Graphical abstract. *Journal of Cleaner Production*. https://doi.org/10.1016/j.jclepro.2018.04.017

Wu, C., Huang, L., Xue, S. G., Huang, Y. Y., Hartley, W., Cui, M. qian, & Wong, M. H. (2017). Arsenic sorption by red mud-modified biochar produced from rice straw. *Environmental Science and Pollution Research*, *24*(22), 18168–18178. https://doi.org/10.1007/s11356-017-9466-7

Yaashikaa, P. R., Kumar, P. S., Varjani, S., & Saravanan, A. (2020). A critical review on the biochar production techniques , characterization , stability and applications for circular bioeconomy. *Biotechnology Reports*, *28*, e00570. https://doi.org/10.1016/j.btre.2020.e00570

Yadav, K., & Jagadevan, S. (2020). Influence of Process Parameters on Synthesis of Biochar by Pyrolysis of Biomass: An Alternative Source of Energy. *Recent Advances in Pyrolysis*, 1–14. https://doi.org/10.5772/intechopen.88204

Yadav, M., & Yadav, H. S. (2015). Applications of ligninolytic enzymes to pollutants, wastewater, dyes, soil, coal, paper and polymers. *Environmental Chemistry Letters*, *13*(3), 309–318. https://doi.org/10.1007/s10311-015-0516-4

Yahya, M. D., Obayomi, K. S., Abdulkadir, M. B., Iyaka, Y. A., & Olugbenga, A. G. (2020). Characterization of cobalt ferrite-supported activated carbon for removal of chromium and

lead ions from tannery wastewater via adsorption equilibrium. *Water Science and Engineering*, *13*(3), 202–213. https://doi.org/10.1016/j.wse.2020.09.007

Yang, H. M., Zhang, D. H., Chen, Y., Ran, M. J., & Gu, J. C. (2017). Study on the application of KOH to produce activated carbon to realize the utilization of distiller's grains. *IOP Conference Series: Earth and Environmental Science*, *69*(1), 0–8. https://doi.org/10.1088/1755-1315/69/1/012051

Yang, X., Ng, W., Wong, B. S. E., Baeg, G. H., Wang, C. H., & Ok, Y. S. (2019). Characterization and ecotoxicological investigation of biochar produced via slow pyrolysis: Effect of feedstock composition and pyrolysis conditions. *Journal of Hazardous Materials*, *365*(February 2018), 178–185. https://doi.org/10.1016/j.jhazmat.2018.10.047

Yavari, S., Malakahmad, A., Sapari, N. B., & Yavari, S. (2017). Sorption properties optimization of agricultural wastes-derived biochars using response surface methodology. *Process Safety and Environmental Protection*, *109*, 509–519. https://doi.org/10.1016/j.psep.2017.05.002

Yeddou, N., & Bensmaili, A. (2007). Equilibrium and kinetic modelling of iron adsorption by eggshells in a batch system: effect of temperature. *Desalination*, *206*(1–3), 127–134. https://doi.org/10.1016/j.desal.2006.04.052

Yu, J., Jiang, C., Guan, Q., Ning, P., Gu, J., Chen, Q., Zhang, J., & Miao, R. (2018). Enhanced removal of Cr(VI) from aqueous solution by supported ZnO nanoparticles on biochar derived from waste water hyacinth. *Chemosphere*, *195*, 632–640. https://doi.org/10.1016/j.chemosphere.2017.12.128

Yuan, Y., Bolan, N., Prévoteau, A., Vithanage, M., Biswas, J. K., Ok, Y. S., & Wang, H. (2017). Applications of biochar in redox-mediated reactions. *Bioresource Technology*, *246*, 271–281. https://doi.org/10.1016/j.biortech.2017.06.154

Zaker, A., Chen, Z., Wang, X., & Zhang, Q. (2019). Microwave-assisted pyrolysis of sewage sludge: A review. *Fuel Processing Technology*, *187*(August 2018), 84–104. https://doi.org/10.1016/j.fuproc.2018.12.011

Zeng, X., Sun, X., Yu, Y., Wang, H., & Wang, Y. (2019). Photocatalytic degradation of flumequine with B/N codoped TiO2 catalyst: Kinetics, main active species, intermediates and pathways. *Chemical Engineering Journal*, *378*(June), 122226. https://doi.org/10.1016/j.cej.2019.122226

Zhang, A., Li, X., Xing, J., & Xu, G. (2020). Adsorption of potentially toxic elements in water by modified biochar: A review. *Journal of Environmental Chemical Engineering*, *8*(4), 104196. https://doi.org/10.1016/j.jece.2020.104196

Zhang, Y., Jin, B., Ma, B., & Feng, X. (2017). Separation of indium from lead smelting hazardous dust via leaching and solvent extraction. *Journal of Environmental Chemical Engineering*, *5*(3), 2182–2188. https://doi.org/10.1016/j.jece.2017.04.034

Zhou, Q., Liao, B., Lin, L., Qiu, W., & Song, Z. (2018). Adsorption of Cu(II) and Cd(II) from aqueous solutions by ferromanganese binary oxide–biochar composites. *Science of the Total Environment*, *615*, 115–122. https://doi.org/10.1016/j.scitotenv.2017.09.220

Zhou, R., Zhang, M., Li, J., & Zhao, W. (2020). Optimization of preparation conditions for

biochar derived from water hyacinth by using response surface methodology (RSM) and its application in Pb2+removal. *Journal of Environmental Chemical Engineering*, *8*(5), 104198. https://doi.org/10.1016/j.jece.2020.104198

Appendix

Appendix A: Thermal analysis result (TGA) raw water hyacinth sample

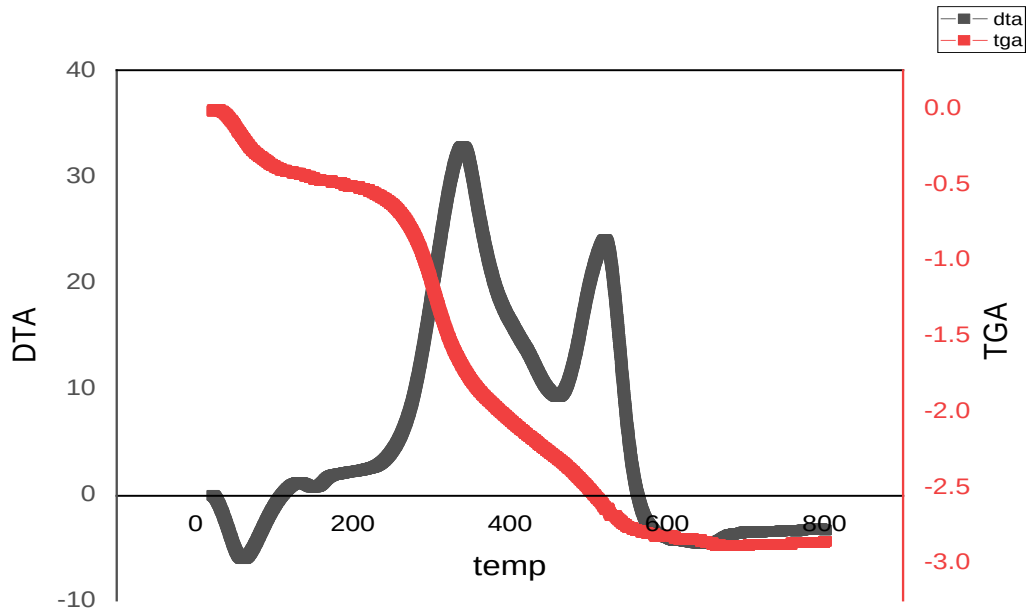

Appendix B: Proximate Analysis of water hyacinth and water hyacinth biochar (BBC) at 500 ^{o}C.

Material	Proximate analysis	Value
Raw water hyacinth	Moisture content, %M	10.87
	Percentage volatile matter, %VM.	65.13
	Percentage ash content, %Ash.	16.3
	Percentage fixed carbon content, %FC.	18.57

Appendix C: Isotherm data for the removal of iron by KOH-WHBC

Experimental data of adsorption for Langmuir isotherm

Exp. no	**C_i(mg/L)**	**C_e(mg/L)**	**q_e(mg/g)**	**C_e/q_e**
1	10	2.5	1.66	1.566

2	20	5	3.25	1.58
3	30	7	4.54	1.63
4	40	8.5	5.17	1.66
5	50	11.7	7.51	1.684
6	60	13.25	8.48	1.715
7	70	15	9.55	1.74
8	80	18.5	11.7	1.782

Experimental data of adsorption for freundlich isotherm

Exp. no	**C_i(mg/L)**	**C_e(mg/L)**	**lnC_e (mg/L)**	**lnq_e(mg/L)**
1	10	2.5	0.92	3.63
2	20	5	1.61	3.84
3	30	7	1.95	3.95
4	40	8.5	2.14	4.01
5	50	11.7	2.46	4.1
6	60	13.25	2.58	4.14
7	70	15	2.71	4.18
8	80	18.5	2.92	4.24

Appendix D: Pseudo-first order and pseudo-second order kinetics data and its constant values

Time(min)	**Co (mg/L)**	**ln(qe-qt)**	**t/qt (g.min/mg)**
50	1	2.7313	0.8193
100	1	2.41	1.556
150	1	2.09	2.29
200	1	1.77	3.03
250	1	1.45	3.767

Appendix E: Standard calibration curve of phosphate removal

a) Ph meter b)reagent bottle c) Stock iron solution d) Standard iron solution

e) Mixing the adsorbent with sample f) after adsorption is takes place

Appendix F: Sample preparation from water hyacinth

Raw water hyacinth

Root of water hyacinth

Washed root water

Dried in an oven at 105 ^{O}C for 24 hour

Final product of water

Sieved with a size of (1.0 to 2.0 mm)

Further grinded with grinder

Appendix G: Synthesize of water hyacinth derived biochar (WHBC)

Dried water hyacinth

Calcination (Muffle furnace) at (300- 700 ^{o}C)

Conserved in a desiccator

Sieved with a size of (250–355 µm).

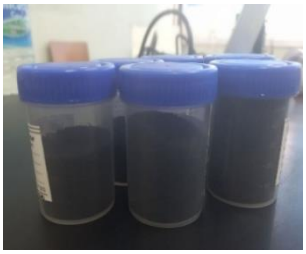

Appendix H: Activation of water hyacinth-derived biochar (WHBC) by KOH

Potassium hydroxide (KOH)

Biochar

Biochar + KOH

Stirred by magnetic stirrer for 2hr at 90 ^{0}C

Filtered by vacuum filter

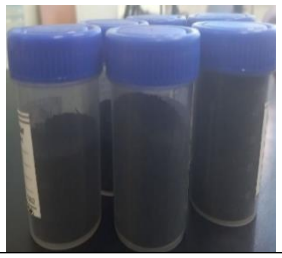

Sample stored for adsorption and characterization

Grounded in mortal and pestle

Oven dried at 110 ^{0}C for 24 hr

Appendix I: Point zero charge analysis of activated water hyacinth biochar

50ml of iron solution is prepared in different Erlenmeyer flask

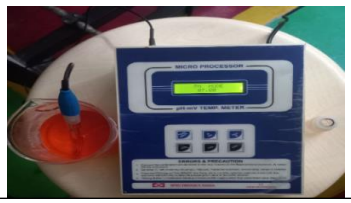

pH of the solution (3-10) was set with HCl and NaOH (0.1M) Solution

0.5g was measured and added to the solution

The final pH value were recorded of the filtrates accordingly

Filtered the content

Shacked the flask at speed of 150 rpm at 25 ^{0}C for 24

Appendix J: Waste water analysis (for chromium, iron and manganese)

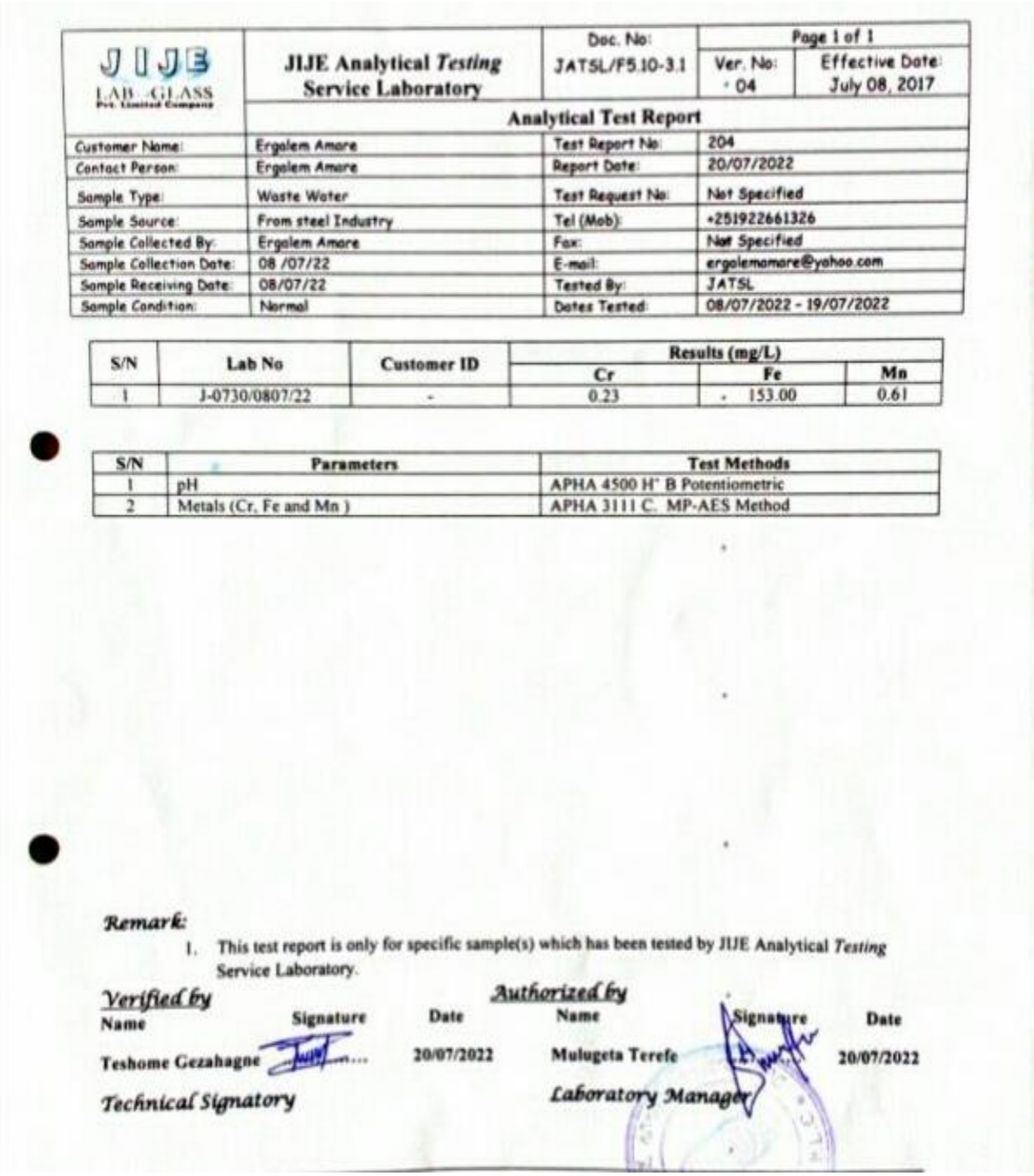

JIJE LAB GLASS Pvt. Limited Company	JIJE Analytical *Testing* Service Laboratory	Doc. No: JATSL/F5.10-3.1	Page 1 of 1	
			Ver. No: 04	Effective Date: July 08, 2017

Analytical Test Report

Customer Name:	Ergalem Amare	Test Report No:	204
Contact Person:	Ergalem Amare	Report Date:	20/07/2022
Sample Type:	Waste Water	Test Request No:	Not Specified
Sample Source:	From steel Industry	Tel (Mob):	+251922661326
Sample Collected By:	Ergalem Amare	Fax:	Not Specified
Sample Collection Date:	08 /07/22	E-mail:	ergalemamare@yahoo.com
Sample Receiving Date:	08/07/22	Tested By:	JATSL
Sample Condition:	Normal	Dates Tested:	08/07/2022 - 19/07/2022

S/N	Lab No	Customer ID	Results (mg/L)		
			Cr	Fe	Mn
1	J-0730/0807/22	-	0.23	153.00	0.61

S/N	Parameters	Test Methods
1	pH	APHA 4500 H+ B Potentiometric
2	Metals (Cr, Fe and Mn)	APHA 3111 C. MP-AES Method

Remark:

1. This test report is only for specific sample(s) which has been tested by JIJE Analytical *Testing* Service Laboratory.

Verified by			*Authorized by*		
Name	Signature	Date	Name	Signature	Date
Teshome Gezahagne		20/07/2022	Mulugeta Terefe		20/07/2022
Technical Signatory			*Laboratory Manager*		

Source : (Kibret & Science, 2023)

Appendix K: Waste water analysis (for copper, nickel and lead)

Company Name

በኢትዮጵያ የኮንስትራክሽን ዲዛይንና ሱፐርቪዥን ሥራዎች ኮርፖሬሽን

Ethiopian Construction Design & Supervision Works Corporation

Tel: - 251-11-872-3643/ - 251-11-872-3478/- 251-11-869-5125/- 251-11-872-1236

Fax - 251-11- P.O.Box 2561 E-mail info@ecdswc.com

Title:		Document No:	Issue No. 1	Page No.
Water Quality Test Report		OF/ECDSW C/0941		1 of 2

Lab No.:- 238/2015 Client Ref: - Lab /02/W/105/22

Client/Project: - Ergalem Amare Date Collected: - -

Client ID:- Source of Sample:- Waste

Location:- Steel Industy Waste Water Date Received:- 2/9/2022

Date Reported :- 19/9/2022

No	Tests	Test Results	Unit	Test Method	WHO maximum allowable Concentration (mg/L)
1	Copper(Cu)	ND	mg/L	Flame AAS	2.0
2	Nickel	ND	mg/L	Flame AAS	3
3	Lead (pb)	ND	mg/L	Flame AAS	0.01

REMARK:-1. The test result can be compared with the WHO maximum allowable concentration (mg/L) presented on the right column. The water sample is collected and submitted to the laboratory by the client.

2. ND = Not detected

Reported by Lab Expert

Checked by Senior Water Quality Expert

Approved by Water Quality S/P Manager

Among the major services rendered by the Water Quality Laboratory Testing S/Process of Ethiopian Construction Design & Supervision Works Corporation are Testing all the Physico-Chemical and Bacteriological analysis of potable or drinking water/ Bottled drinking water/, waste water, water for construction and irrigation uses and sampling of water and waste water.

Please make sure that this document is the correct version before use

Source : (Kibret & Science, 2023)

Appendix L: Brunauer-Emmett-Teller (BET) Analysis result

Quantachrome NovaWin - Data Acquisition and Reduction
for NOVA instruments
©1994-2010, Quantachrome Instruments
version 11.0

Analysis		Report	
Operator:alex	Date:2007/01/01	Operator:alex	Date:1/3/2024
Sample ID: sof 1	Filename:	C:\QCdata\Physisorb\sofia 1.qps	
Sample Desc: sample	Comment:	TEST	
Sample weight: 0.05 g	Sample Volume:	0.01282 cc	Sample Density:3.9 g/cc
Outgas Time: 8.0 hrs	OutgasTemp:	300.0 C	
Analysis gas: Nitrogen	Bath Temp:	77.3 K	
Press. Tolerance:0.100/0.100 (ads/des)	Equil time:	60/60 sec (ads/des)	Equil timeout: 240/240 sec (ads/des)
Analysis Time: 54.5 min	End of run:	2007/01/01 1:22:10	Instrument: Nova Station B
Cell ID: 2			F/W version: 0.00
Adsorbate Nitrogen	Temperature	77.350K	
Molec. Wt.: 28.013 g	Cross Section:	16.200 Ų	Liquid Density: 0.808 g/cc

Relative Pressure P/Po	Volume @ STP cc/g	1 / [W((Po/P) - 1)]
5.16850e-02	18.4448	2.3642e+00
1.21626e-01	41.8308	2.6485e+00
2.09720e-01	70.6094	3.0071e+00
2.73666e-01	91.2460	3.3039e+00
3.47292e-01	114.9643	3.7031e+00

BET summary

Slope =	4.477
Intercept =	2.106e+00
Correlation coefficient, r =	0.997895
C constant=	3.126

Surface Area = 528.964 m²/g